Accepted Manuscript

Discovery, synthesis and anti-atherosclerotic activities of a novel selective sphingomyelin synthase 2 inhibitor

Yali Li, Taomin Huang, Bin Lou, Deyong Ye, Xiangyu Qi, Xiaoxia Li, Shuang Hu, Tingbo Ding, Yan Chen, Yang Cao, Mingguang Mo, Jibin Dong, Min Wei, Yong Chu, Huiti Li, Xian-Cheng Jiang, Nengneng Cheng, Lu Zhou

PII: S0223-5234(18)31065-1

DOI: https://doi.org/10.1016/j.ejmech.2018.12.028

Reference: EJMECH 10961

To appear in: *European Journal of Medicinal Chemistry*

Received Date: 31 August 2018

Revised Date: 11 December 2018

Accepted Date: 12 December 2018

Please cite this article as: Y. Li, T. Huang, B. Lou, D. Ye, X. Qi, X. Li, S. Hu, T. Ding, Y. Chen, Y. Cao, M. Mo, J. Dong, M. Wei, Y. Chu, H. Li, X.-C. Jiang, N. Cheng, L. Zhou, Discovery, synthesis and anti-atherosclerotic activities of a novel selective sphingomyelin synthase 2 inhibitor, *European Journal of Medicinal Chemistry* (2019), doi: https://doi.org/10.1016/j.ejmech.2018.12.028.

Discovery, synthesis and anti-atherosclerotic activities of a novel selective sphingomyelin synthase 2 inhibitor

Yali Li [a,b,#], Taomin Huang [a,c,#], Bin Lou [a,#], Deyong Ye [a], Xiangyu Qi [a], Xiaoxia Li [a], Shuang Hu [a], Tingbo Ding [a], Yan Chen [a], Yang Cao [a], Mingguang Mo [a], Jibin Dong [a], Min Wei [a], Yong Chu [a], Huiti Li [a], Xian-Cheng Jiang [a,d,*], Nengneng Cheng [a,*], Lu Zhou [a,*]

[a] *School of Pharmacy, Fudan University, No.826, Zhangheng Rd., Shanghai 201203, China*

[b] *Institute for Agro-food Standards and Testing Technology, Shanghai Academy of Agricultural Sciences, No.1000, Jinqi Rd., Shanghai 201403, China*

[c] *Eye Ear Nose Throat Hospital, Fudan University, No. 83, Fenyang Rd., Shanghai 200031, China*

[d] *State University of New York Downstate Medical Center, Brooklyn, New York 11203, USA*

Graphical abstracts

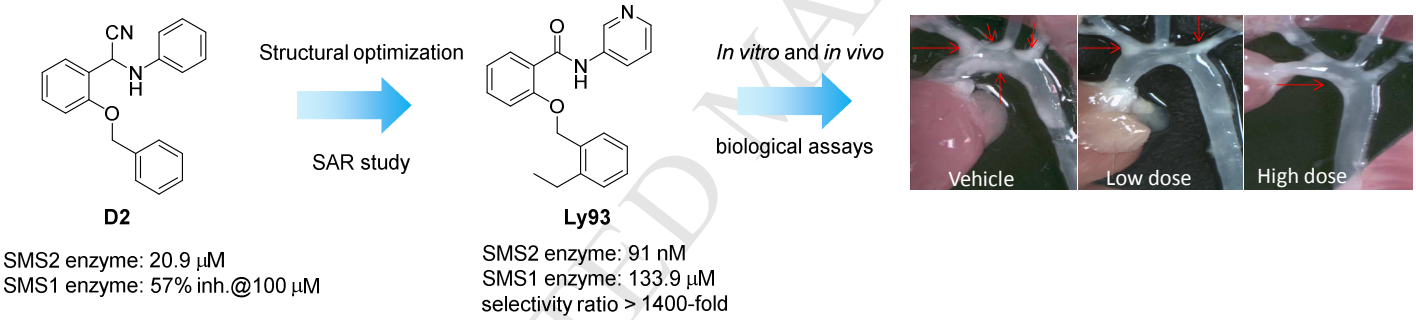

Discovery of a 2-benzyloxybenzamide Ly93 as a novel selective SMS2 inhibitor and the studies on its *in vitro* and *in vivo* biological activities

Discovery, synthesis and anti-atherosclerotic activities of a novel selective sphingomyelin synthase 2 inhibitor

Yali Li [a,b,#], Taomin Huang [a,c,#], Bin Lou [a,#], Deyong Ye [a], Xiangyu Qi [a], Xiaoxia Li [a], Shuang Hu [a], Tingbo Ding [a], Yan Chen [a], Yang Cao [a], Mingguang Mo [a], Jibin Dong [a], Min Wei [a], Yong Chu [a], Huiti Li [a], Xian-Cheng Jiang [a,d,*], Nengneng Cheng [a,*], Lu Zhou [a,*]

[a] *School of Pharmacy, Fudan University, No.826, Zhangheng Rd., Shanghai 201203, China*
[b] *Institute for Agro-food Standards and Testing Technology, Shanghai Academy of Agricultural Sciences, No.1000, Jinqi Rd., Shanghai 201403, China*
[c] *Eye Ear Nose Throat Hospital, Fudan University, No. 83, Fenyang Rd., Shanghai 200031, China*
[d] *State University of New York Downstate Medical Center, Brooklyn, New York 11203, USA*

ABBREVIATIONS

SM, sphingomyelin; SMS, sphingomyelin synthase; SMS2, sphingomyelin synthase 2; PC, phosphatidylcholine; SPT, serine palmitoyltransferase; AS, atherosclerosis; IC_{50}, 50% inhibiting concentration; apoB, apolipoprotein B; apoE, apolipoprotein E; KO, knock out; HPLC, high-performance liquid chromatography.

[#] These authors contributed equally to this work. *****Correspondence should be addressed to: Tel. +1-718 270 6701. *E-mail address*: xjiang@downstate.edu (X Jiang); *E-mail address*: chengnn@163.com (N Cheng); Tel. & Fax: +86-21-51980125. *E-mail address*: zhoulu@fudan.edu.cn (L Zhou).

Abstract

The sphingomyelin synthase 2 (SMS2) is a potential target for pharmacological intervention in atherosclerosis. However, so far, few selective SMS2 inhibitors and their pharmacological activities were reported. In this study, a class of 2-benzyloxybenzamides were discovered as novel SMS2 inhibitors through scaffold hopping and structural optimization. Among them, Ly93 as one of the most potent inhibitors exhibited IC_{50} values of 91 nM and 133.9 μM against purified SMS2 and SMS1 respectively. The selectivity ratio of Ly93 was more than 1400-fold for purified SMS2 over SMS1. The *in vitro* studies indicated that Ly93 not only dose-dependently diminished apoB secretion from Huh7 cells, but also significantly reduced the SMS activity and increased cholesterol efflux from macrophages. Meanwhile, Ly93 inhibited the secretion of LPS-mediated pro-inflammatory cytokine and chemokine in macrophages. The pharmacokinetic profiles of Ly93 performed on C57BL/6J mice demonstrated that Ly93 was orally efficacious. As a potent selective SMS2 inhibitor, Ly93 significantly decreased the plasma SM levels of C57BL/6J mice. Furthermore, Ly93 was capable of dose-dependently attenuating the atherosclerotic lesions in the root and the entire aorta as well as macrophage content in lesions, in apolipoprotein E gene knockout mice treated with Ly93. In conclusion, we discovered a novel selective SMS2 inhibitor Ly93 and demonstrated its anti-atherosclerotic activities *in vivo*. The preliminary molecular mechanism-of-action studies revealed its function in lipid homeostasis and inflammation process, which indicated that the selective inhibition of SMS2 would be a promising treatment for atherosclerosis.

***Keywords*:**

Sphingomyelin synthase 2; Inhibitor; ApoE KO mice; Atherosclerosis.

1. Introduction

Sphingomyelin (SM) is one of the major phospholipids in the circulation [1]. It has been proved that human plasma SM levels are an independent risk factor for coronary heart disease [2, 3] and prognostic in patients with acute coronary syndrome [3]. In apoE KO mice, the plasma SM levels that are four-fold higher than those in control mice [4]. The raised plasma SM could further induce the increased atherosclerosis found in these animals [5]. Meanwhile, SM that are enriched in atherogenic lipoproteins has significant effects on the metabolism of apoB-containing lipoproteins [1, 6]. The deficiency of SM in atherogenic lipoproteins could reduce the atherogenic properties of the mice [7].

Moreover, SM is also one of the major phospholipids in the plasma membrane. Macrophages, as the most prominent cell types in atherosclerotic lesions, are associated with two hallmarks of atherosclerosis involving the formation of foam cells due to excessive accumulation of cholesterol by macrophages [8] and inflammation [1, 9]. Studies on the membrane SM of macrophages revealed that membrane SM could play an important role in the development of atherosclerosis [10-12]. The SM level of macrophage membrane is closely related to the cholesterol efflux and inflammatory responses in macrophages [10, 13]. Thus, the inhibition of SM biosynthesis could directly reduce SM levels not only in atherogenic lipoproteins but also in the membrane of macrophages.

The reduction of SM, with concomitant reduction of atherosclerosis, could be achieved by pharmacologically inhibiting serine palmitoyltransferase (SPT) in mice models, which is the first enzyme for SM biosynthesis [14, 15]. However, the inhibition of SPT could influence the whole sphingolipid *de novo* synthesis pathway and induce many off-target side effects. Therefore, the inhibition of sphingomyelin synthase (SMS) is an alternative approach for the reduction of SM.

SMS is the last enzyme in the SM biosynthetic pathway. It catalyzes the

conversion of ceramide to SM. The SMS gene family consists of three members including SMS1, SMS2 and SMS related protein (SMSr). Both SMS1 and SMS2, but not SMSr, have the SMS catalytic activity [16, 17]. In our previous studies, SMS1 and SMS2 are proved to be the two factors that influence plasma SM levels [7, 11, 18]. Both SMS1 and SMS2 KO mice have lower SM levels in all the tested tissues [11]. However, in the SMS1 knockdown T cells, the TCR signaling was impaired through the dysfunction of lipid rafts [19]. Meanwhile, the SMS1 KO mice exhibited moderate neonatal lethality [11, 20], mitochondrial dysfunction and the increased oxidative stress, which could cause lipodystrophy and impair the insulin secretion from pancreas [20, 21]. Furthermore, the deficiency of SMS1 but not SMS2 could cause hearing impairments in mice. As to the side effects of SMS1 deficiency, the inhibition of SMS2 is an optimal strategy for the reduction of SM level.

Our studies have already indicated that the SMS overexpression could promote the accumulation of atherogenic lipoprotein and increase atherogenic potential [22]. Contrarily, the SMS deficiency reduces the SM accumulation and thereby alleviates atherosclerosis in a mouse model [10-12]. These intriguing findings raise the possibility that SMS2 is a potential therapeutic target of atherosclerosis. The selective SMS2 inhibitors are likely to be developed as anti-atherosclerotic drugs. However, the impact of selective SMS2 inhibition on the development of atherosclerosis has not been investigated so far due to the lack of potent selective SMS2 inhibitors.

Up to date, very few selective SMS2 inhibitors have been reported in the literature. **D609** (**Fig. 1**), firstly discovered as an anti-tumor agent [23, 24], was reported with weak SMS inhibitory activity *in vitro* (IC_{50} = 177-600 μM) [25-27]. The α-aminonitrile derivatives were the first series of SMS inhibitors discovered through rational drug design by our research group. The representative compound **D2** (**Fig. 1**) has an IC_{50} value of 24.5 μM for SMS from liver homogenate of ICR mice and an IC_{50} value of 13.5 μM for SMS2 over-expressed insect cell lysis [28, 29]. However, the latently toxigenic α-aminonitrile group of compound **D2** precluded the further

application in the *in vivo* medication of atherosclerosis. SAPA derivatives (**Fig. 1**) were then discovered as a novel class of SMS1 inhibitors with micromolar inhibitory activities against SMS1 over-expressed Hela cell lysis [30]. However, the effects of **SAPA 1j** on SMS2 had not been explored. Furthermore, oxazolopyridine derivatives (**Fig. 1**) were designed and firstly tested the inhibitory activity towards purified SMS2. Among them, the compound **QY10** possess an IC_{50} value of 1.7 μM against purified SMS2 enzyme [31]. Moreover, a 2-quinolone derivative (**Fig. 1**) was identified as a potent SMS2 selective inhibitor (IC_{50} = 16 nM for SMS2 over-expressed membrane fraction), of which the *in vitro* and *in vivo* biological activities were not reported [32]. 4-Benzyloxybenzo[*d*]isoxazole-3-amine derivatives were discovered as potent SMS2 selective inhibitors. The most promising representative compound (**Fig. 1**) was found to be with IC_{50} values of 0.10 μM against SMS2 and 56 μM against SMS1 [33].

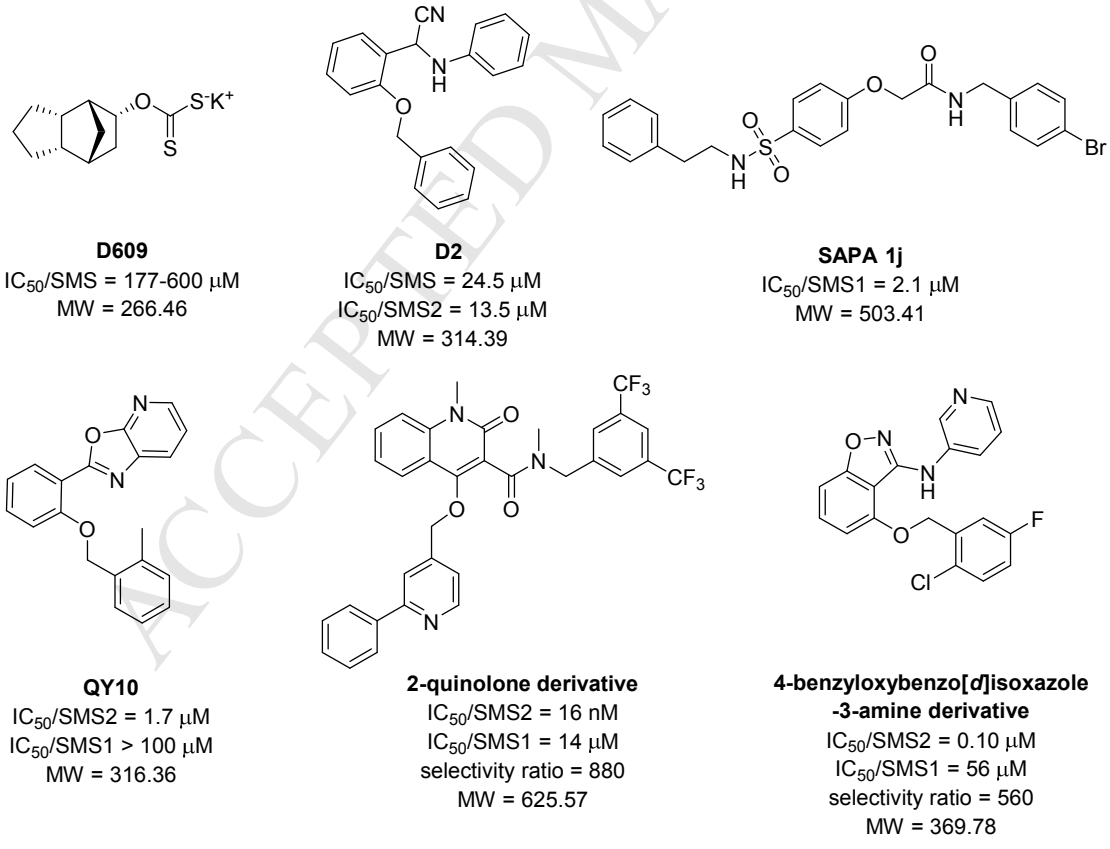

Fig 1. Chemical structures of reported sphingomyelin synthase inhibitors.

In the current study, 2-(benzyloxy)-*N*-arylbenzamide derivatives were

discovered as a novel series of SMS2 inhibitors. The representative compound Ly93 was proved with the selectivity ratio of more than 1400-fold for purified SMS2 over SMS1. The *in vitro* biological evaluations were performed on Ly93 for the exploration of the potential anti-atherosclerotic mechanisms. Finally, Ly93 was put into the *in vivo* studies and exhibited significant anti-atherosclerotic activities in apoE KO mice. The research in this paper indicated that the selective inhibition of SMS2 would be a promising treatment for atherosclerosis.

2. Experiments and Results

2.1 The discovery of 2-benzyloxybenzamides as novel SMS2 inhibitors.

Although the α-aminonitrile group of **D2** could play a role in the inhibition of SMS based on the docking model of *h*SMS1 [28], the latent toxigenicity of α-aminonitrile precluded the further application of **D2** in the *in vivo* medication of atherosclerosis. Thus, as shown in **Fig. 2**, scaffold hopping was firstly conducted on the α-aminonitrile group (section A) of the previously reported SMS2 inhibitor **D2** [28] to eliminate the potential toxigenic effects of the lead compound **D2**. The detailed approaches of scaffold hopping were shown in **Supplementary Fig. 1**. The compounds derived from **D2** were then validated by the SMS2 inhibition assay using SMS2 over-expressed insect cell lysate. As shown in **Supplementary Table 1**, only the compound **D2-e** retained the SMS2 inhibitory activity with the IC_{50} value of 13.4 μM, while the other compounds **D2-a**, **b**, **c**, **d** were less potent. The results indicated that the amide group of **D2-e**, similar to the α-aminonitrile group, could accommodate to the steric restriction and the electronic effects of the binding site [28]. It was also estimated that the amide group (section A) of **D2-e** might be vital for the SMS2 inhibition as well as for the improved physicochemical property. Based on the docking model of **D2-e** with *h*SMS2 which was derived from the previously reported model of *h*SMS1 [34], the further chemical modifications were performed on the section B to investigate the structure and activity relationship

(SAR). Finally, as the benzyl group was located at the position between two helixes with space tolerance, substitutes with different electronic and steric effects were introduced onto the benzene ring to explore the SAR of the section C and discover more potent and selective SMS2 inhibitors.

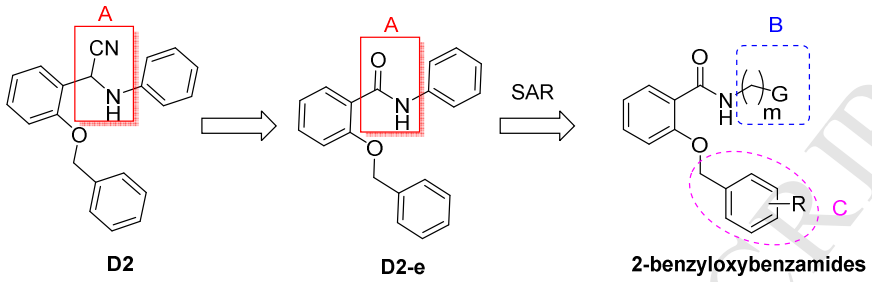

Fig 2. The design strategy and SAR study of 2-benzyloxybenzamides as novel SMS2 inhibitors.

2.2 The synthesis of novel 2-benzyloxybenzamides.

2-benzyloxybenzamides **6-11** were firstly designed to investigate the SAR of the section B of the compound **D2-e.** Compounds **6-11** were synthesized according to the **Scheme 1**. Intermediates **3a** and **3b** were synthesized through the nucleophilic substitution reaction of methyl salicylate **1** with benzyl bromide **2a** and **2b** respectively. Then **3a** and **3b** were hydrolyzed to give 2-benzyloxybenzoic acid **4a** and **4b** respectively. The **4a** was reacted with thionyl chloride and amine **5a**, **5b**, **5d** or **5e** sequentially to give **6**, **7**, **9** and **10**. Compound **8** was prepared through the condensation of **4a** with cyclohexanamine **5c**. Compound **11** was obtained from the condensation of **4b** with *N*-boc-piperidin-3-amine **5f** and subsequently the deprotection of the Boc group.

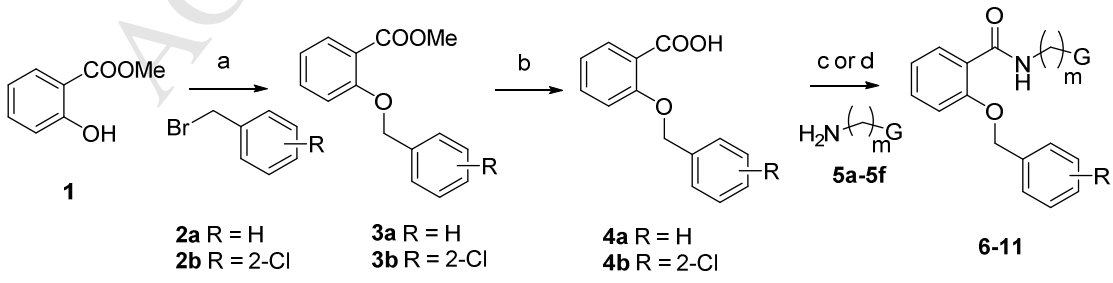

Scheme 1. The synthetic route for 2-benzyloxybenzamides 6-11. Reagents and conditions: (a) K_2CO_3, acetone, rt; (b) 1) 4 M NaOH (aq), CH_3OH; 2) 2M HCl (aq);

(c) 1) $SOCl_2$, Pyridine (cat.), reflux; 2) Pyridine, CH_2Cl_2, 0 ^oC to rt; (d) 1) EDCI, DMAP, CH_2Cl_2, 0 ^oC to rt; 2) HCl (aq, con.), EA.

2-benzyloxybenzamides **19-45** were designed to investigate the SAR of the section C of the compound **10**. Compounds **19-45** were synthesized according to the **Scheme 2**. The key intermediate **12** was prepared through the debenzylation of compound **10** under the hydrogen and catalytic palladium. **15c** and **15d** were synthesized through the nucleophilic substitution of 5-chlorosalicylic aldehyde **13** with bromoalkane. Commercially available reagents **15a** and **15b** coupled with **15c** and **15d** were reacted with sodium borohydride to give the benzyl alcohol **17a-17d**. Meanwhile, intermediate **14a** was obtained from the reduction of **13** by sodium borohydride and then with salicylic alcohol **14b** to afford benzyl alcohol **17j-17n**. Commercially available benzoic acids **16a-16e** were reacted with borane in tetrahydrofuran to give benzyl alcohol **17e-17i**. Benzyl bromides **18k-18x** was prepared from the bromination of benzyl alcohols **17a-17n** with phosphorus tribromide, and subsequently with the commercially available reagents **18a-18j** provided the target compounds **19-22 (the compound 22 was named as Ly93)**, **24-33** and **36-45** by reacting with the key intermediate **12**. Finally, benzyl alcohols **17o-17q** directly provided the target compounds **23**, **34** and **35** through the Mitsunobu reaction with **12**.

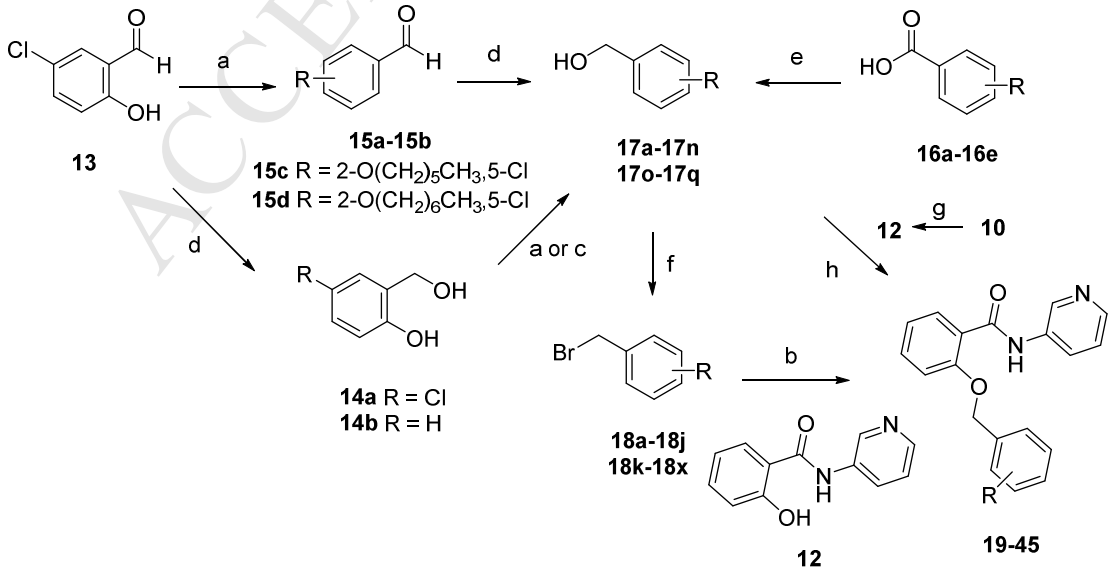

Scheme 2. The synthetic route for 2-benzyloxybenzamides 19-45. Reagents and conditions: (a) K_2CO_3, CH_3CN, 60 ^oC; (b) K_2CO_3, acetone, rt; (c) K_2CO_3, DMF, 100 ^oC; (d) $NaBH_4$, C_2H_5OH, 0 ^oC to rt; (e) BH_3, THF, 0 ^oC to rt; (f) PBr_3, CH_2Cl_2, 0 ^oC to rt; (g) H_2, 10% Pd/C, CH_3OH, rt; (h) DEAD, Ph_3P, THF, 0 ^oC to rt.

The structures of all newly synthesized compounds were elucidated from their analytical and spectroscopic data which were collected in the **Material and Methods** and **Supplementary Material**.

2.3 The in vitro SMS2 inhibitory activities of novel 2-benzyloxybenzamides.

All the newly prepared compounds were further evaluated the SMS2 inhibitory activities on the SMS2 over-expressed insect cell lysate. The SMS2 inhibitory activities of 2-benzyloxybenzamides were shown in **Table 1**. The results revealed that 27 compounds were more potent SMS2 inhibitors than D2-e (IC_{50} = 13.4 μM). Among them, 11 compounds exhibited robust SMS2 inhibitory activities with the IC_{50} values lower than 1 μM. Compound **45** with the IC_{50} value of 0.43 μM was most effective than other 2-benzyloxybenzamides on the SMS2 inhibition.

Table 1. The SMS2 inhibitory activities of 2-benzyloxybenzamides 6-11 and 19-45.

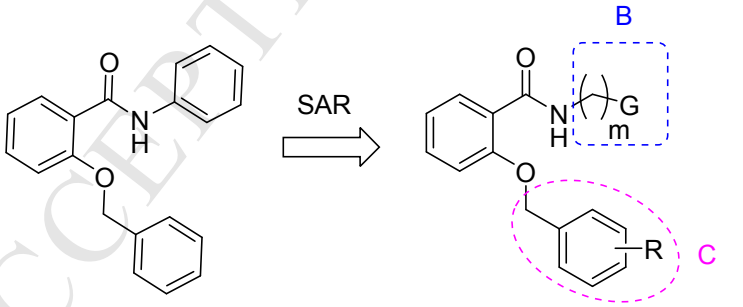

D2-e

2-benzyloxybenzamides
6-11, 19-45

Compd.	G	m	R	SMS2 IC_{50} (μM)[a]
D2				13.5

D2-e	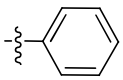	0	-H	13.4
6	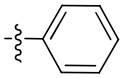	1	-H	34.2
7	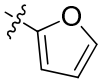	1	-H	49.0
8	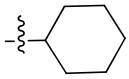	0	-H	43.4
9	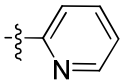	0	-H	11.7
10	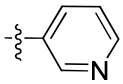	0	-H	3.2
11	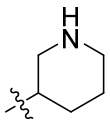	0	2-Cl	> 100
19	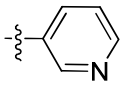	0	2-F	3.5
20	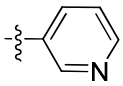	0	2-Cl	1.1
21	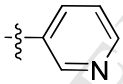	0	2-CH_3	1.5
22 (Ly93)	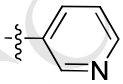	0	2-C_2H_5	0.88
23	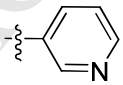	0	2-CF_3	2.1
24	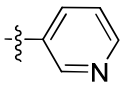	0	2-CN	31.8
25	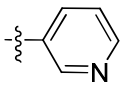	0	3-F	1.6

26	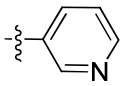	0	3-Cl	1.4
27	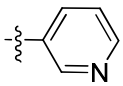	0	3-CN	60.7
28	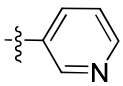	0	2-Cl, 5-F	0.74
29	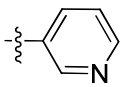	0	2-Cl, 6-F	1.5
30	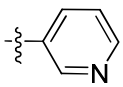	0	2,5-di-Cl	0.99
31	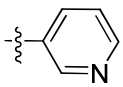	0	2,6-di-Cl	0.69
32	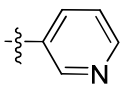	0	2-F, 3-Cl	3.1
33	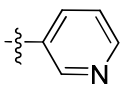	0	2-CH_3, 5-F	0.74
34	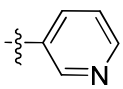	0	2-CH_3, 5-Cl	1.1
35	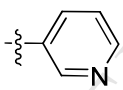	0	2-CH_3, 3-Cl	3.8
36	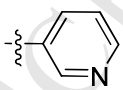	0	2,6-di-CH_3	0.89
37	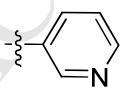	0	2,5-di-OCH_3	2.8
38	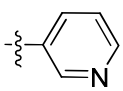	0	2-OCH_3, 5-Cl	0.67
39	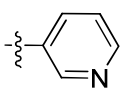	0	2-$O(CH_2)_2OCH_3$, 5-Cl	11.6

40	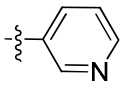	0	2-O$(CH_2)_3OCH_3$, 5-Cl	4.1
41	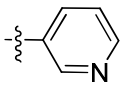	0	2-O$(CH_2)_4$Cl	1.3
42	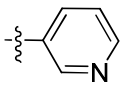	0	2-O$(CH_2)_5$Cl	0.67
43	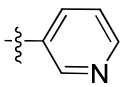	0	2-O$(CH_2)_6$Cl	0.47
44	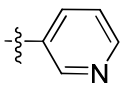	0	2-O$(CH_2)_5CH_3$, 5-Cl	0.52
45	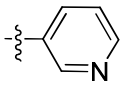	0	2-O$(CH_2)_6CH_3$, 5-Cl	0.43

[a] IC_{50} values are the means of three separate determinations on SMS2 over-expressed insect cell lysate and were determined by more than five concentrations of each inhibitor. Statistical calculation of IC_{50} values was performed on GraphPad Prism 5.02 (GraphPad Software, Inc.).

2.4 The SARs of 2-benzyloxybenzamides as novel SMS2 inhibitors.

In order to explore the interesting enzymatic profile, a preliminary structure-activity relationship of 2-benzyloxybenzamides was analyzed on the basis of *in vitro* enzymatic activities.

The SMS2 inhibitory activities were dramatically reduced by not only the introduction of methylene (**6** *vs* **D2-e**) but also the substitution of phenyl with a saturated ring (**8** *vs* **D2-e**). Compounds **9** and **10** had improved SMS2 inhibitory activities due to the substitution of phenyl with pyridyl. The aromatic group **G** was proved to be crucial for SMS2 inhibition by comparison of **10** with **11**.

Substituent group R was also important for the SMS2 inhibitory activities of 2-benzyloxybenzamides. The SMS2 inhibitory activities were enhanced by the introduction of a chlorine atom (**20**) or an alkyl group (**21**, **22**) onto the ortho-position as well as halogen atoms (**25**, **26**) onto the meta-position. However, the presence of

ortho- or meta- cyano group (**24**, **27**) could dramatically weaken the inhibitory activities toward SMS2. Furthermore, the SMS2 inhibitory potency could be further elevated by the dual substitution of halogen atoms or alkyl groups at 2,5- and 2,6-positions. It exhibited the superimposed effects of advantaged groups. The hydrophobic chain of C4-C7 alkoxy group on the ortho-position (**41**-**45**) were also the advantaged groups for improving the SMS2 inhibitory potency.

The structure-activity relationships achieved by 2-benzyloxybenzamides would be helpful for developing more potent SMS2 inhibitors in the future.

2.5 The in vitro inhibitory activities and selectivity of Ly93 against purified SMS1 and SMS2.

Among the 2-benzyloxybenzamides derivatives shown above, the novel small molecule Ly93 was designed, synthesized and validated (its structural spectra were shown in **Supplementary Fig. 2**), and showed to be one of the most potent SMS2 inhibitors. Due to the distinguished SMS2 inhibitory activity and optimal properties, Ly93 was selected for the further studies. As SMS1 and SMS2 purified enzymes were expressed (unpublished work from Prof Yu Cao), it was possible for us to evaluate the *in vitro* inhibitory activities and selectivity of compound Ly93 against purified SMS1 and SMS2. As a result, as shown in **Fig. 3**, Ly93 exhibited dose-dependent SMS inhibitory activities toward purified SMS1 and SMS2. The IC_{50} values of Ly93 were 91 nM and 133.9 μM toward purified SMS2 and SMS1 respectively. The selectivity ratio of Ly93 was > 1400-fold for purified SMS2 over SMS1. Therefore, Ly93 was proved to be a novel potent selective SMS2 inhibitor.

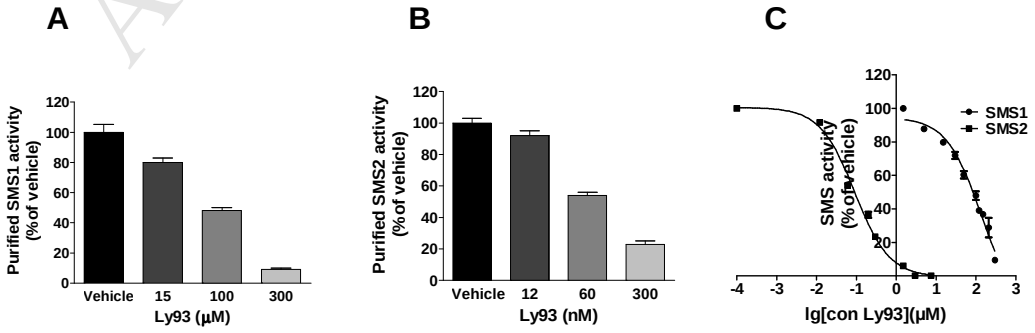

Fig 3. The inhibitory activities of Ly93 against purified SMS1 and SMS2 *in vitro*. (A) The inhibitory activity of Ly93 against purified SMS1 enzyme *in vitro*. (B) The inhibitory activity of Ly93 against purified SMS2 enzyme *in vitro*. The results were expressed as percent of SMS1 or SMS2 activities in vehicle groups in which there is no inhibitor. (C) The dose-dependent inhibitory activities of Ly93 against purified SMS1 and SMS2 enzyme respectively *in vitro*. The IC_{50} value of D2 toward purified SMS2 was 20.9 μM. The inhibitory rate of D2 toward purified SMS1 was 57 % at the concentration of 100 μM. The IC_{50} value of Ly93 toward SMS1 was tested with ten concentrations. The IC_{50} value of Ly93 toward SMS2 was tested with eight concentrations. Values were shown in means ± SD, $n = 3$.

2.6 The molecular docking study.

Molecular docking study was performed to investigate the interaction of Ly93 with *h*SMS2 which was derived from the previously reported model of *h*SMS1 [34] and built through homology modeling. The binding modes of Ly93 with *h*SMS2 were shown in **Fig. 4A**. As it was shown, Ly93 located at the active site of *h*SMS2 which was responsible for SM production and thus blocked the entry of the substrate PC. The key binding forces between Ly93 and *h*SMS2 were hydrophobic, π-π stacking and van der Waals interactions. The central phenyl moiety formed hydrophobic interactions with Ile278 and Leu225. It also formed a π-π stacking interaction with His229 and van der Waals interactions with His270 and His272 respectively. The pyridine ring formed π-π stacking and van der Waals interactions with Tyr281 and Tyr282. Moreover, as Ly93 located close to the helix, the detrimental steric hindrance limited the structural modification. The benzene ring of benzyl group formed a cation-π interaction with Arg286 which could be reinforced by the electron-donating substitution of the benzene ring. Besides, the hydrophobic substitution of the ortho-position on the benzene ring of benzyl group could improve the hydrophobic interaction with Ile263 and thus enhance the inhibitory potency against SMS2. Meanwhile, as the benzene ring of benzyl group was located at the position between

two helixes and the space tolerance was improved, the long alkoxy chain at the ortho-position of the benzene ring could reach the surface of the protein, increase the hydrophobic property and improve the SMS2 inhibitory activities. As shown in **Fig 4B**, Ile278 in *h*SMS2 had a hydrophobic interaction with the central phenyl moiety of Ly93, while Val334 at the same site in *h*SMS1 did not show similar hydrophobic interaction. The conformation of Ly93 could be stabilized by the compact hydrophobic pocket in *h*SMS2. This difference may contribute to the inhibitory selectivity of Ly93 between *h*SMS1 and *h*SMS2. The docking studies were in accordance with the results of enzymatic assay and gave more SAR information of 2-benzyloxybenzamides.

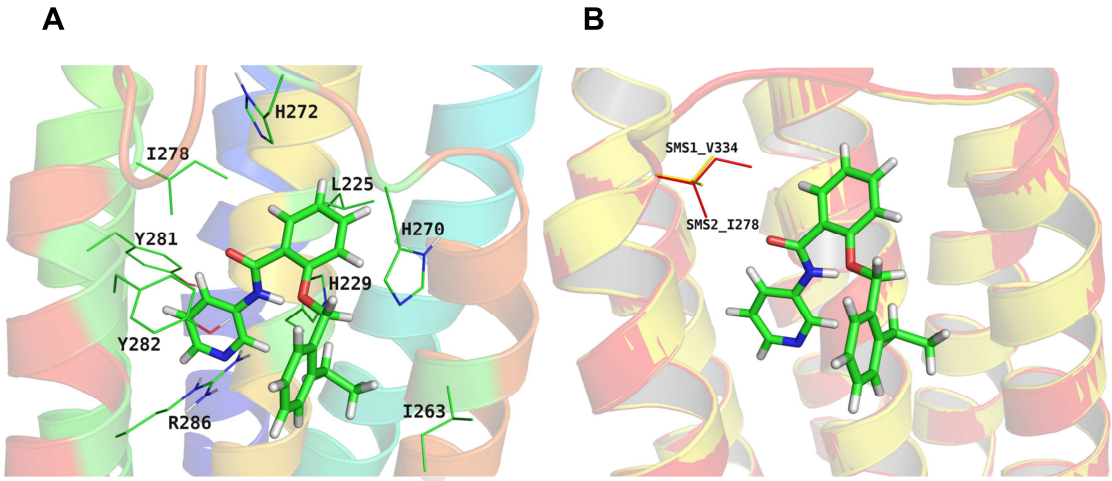

Fig 4. The molecular docking results of Ly93 with *h*SMS2 and *h*SMS1. (A) The binding mode of Ly93 with *h*SMS2. (B) The overlay map of binding modes of Ly93 with *h*SMS1 (yellow) and *h*SMS2 (red). The ribbons in colors stand for the six transmembrane (TM1-TM6) of *h*SMS2 and *h*SMS1. Carbon, oxygen, nitrogen, and hydrogen atoms of the Ly93 molecule are colored green, red, blue and gray, respectively.

In order to investigate the biological actions of selective SMS2 inhibitor, the *in vitro* and *in vivo* biological evaluations were subsequently performed with Ly93.

2.7 The biological effects of Ly93 on the apoB secretion from Huh7 cells, intracellular SMS activity and cholesterol efflux in macrophages.

The secretion of apolipoprotein B (apoB) and the efflux of cholesterol are important processes of cells that are involved in the development of atherosclerosis. ApoB which is synthesized in the liver is acknowledged as an atherogenic lipoprotein. It is also the major protein component of VLDL and chylomicron (CM) in which SM is enriched [1, 6, 35, 36]. In order to investigate the impact of SMS2 inhibition on apoB particle production, Huh7 cells, a human hepatoma cell line, were firstly treated with Ly93. Then apoB secretion from the Huh7 cells was analyzed. As a result, the treatment of Ly93 diminished apoB secretion from Huh7 cells in a dose-dependent manner (**Fig. 5A**). It was suggested that the inhibition of SMS2 in the liver could decrease the production of atherogenic lipoprotein.

As it is known that the cholesterol efflux from macrophages plays an important role in reverse cholesterol transport that is an anti-atherogenic process [37]. In order to study the effects of Ly93 on the cholesterol efflux from macrophages, the bone marrow-derived macrophages were treated with different concentrations of Ly93. As a result, the treatment of Ly93 not only significantly reduced SMS activity (**Fig. 5B**) but also increased the cholesterol efflux in a dose-dependent fashion (**Fig. 5C**).

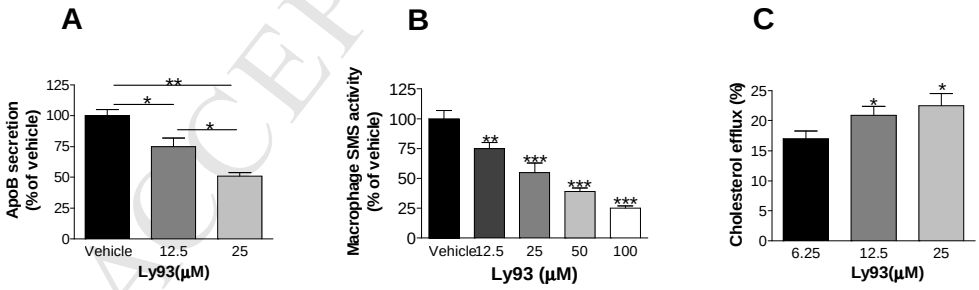

Fig 5. The biological effects of Ly93 on the apoB secretion from Huh7 cells, intracellular SMS activity and cholesterol efflux in macrophages. (A) The effect of Ly93 on the apoB-containing particle secretion from Huh7 cells. Huh7 cells were treated by Ly93 for 17 h and then were labeled with [^{35}S]-methionine in the presence of vehicle or Ly93 for 2 hours. The medium was collected to detect [^{35}S]-apoB and

the quantitation was displayed. (B) Ly93 inhibits macrophage lysate SMS activity in a dose-dependent manner. (C) Ly93 treatment significantly increased macrophage cholesterol efflux toward HDL. Values are mean ± SD, $n = 5$. *$P < 0.05$, **$P < 0.01$, ***$P < 0.001$.

2.8 The in vitro inhibitory activities of Ly93 against the secretion of LPS-mediated pro-inflammatory cytokine and chemokine in macrophages.

Our previous studies have shown that SMS deficiency in macrophages promotes inflammatory responses and subsequently leads to the attenuation of atherosclerosis in mouse models. The mechanism was attributed to the reduced SM levels in plasma membrane lipid rafts [10-12]. Experiments were performed to investigate the effect of the selective SMS2 inhibitor Ly93 on the inflammatory factors of macrophages. Firstly, the production of IL-6 which is a well-known pro-atherogenic cytokine [38] was analyzed when the macrophages were treated with Ly93. As shown in **Fig. 6A**, the treatment of Ly93 could dose-dependently attenuate the LPS-induced IL-6 secretion in macrophages with the comparison of the control. Subsequently, macrophages were pretreated with Ly93 and then stimulated by LPS (50 ng/ml). The activation of NFκB which is a key inflammatory downstream of TLR4 in LPS-induced macrophages was determined. As shown in **Fig. 6B**, the levels of cytosolic IκBα in macrophages were directly increased in a dose-dependent manner by the treatment of Ly93. Thus, the activation of NFκB was indicated to be attenuated by Ly93. Furthermore, the production of MCP-1 which is a pro-inflammatory chemokine was measured in the culture medium of Ly93-treated macrophages. As shown in **Fig. 6C**, the levels of MCP-1 in the culture medium of macrophages were also decreased by the Ly93 treatment.

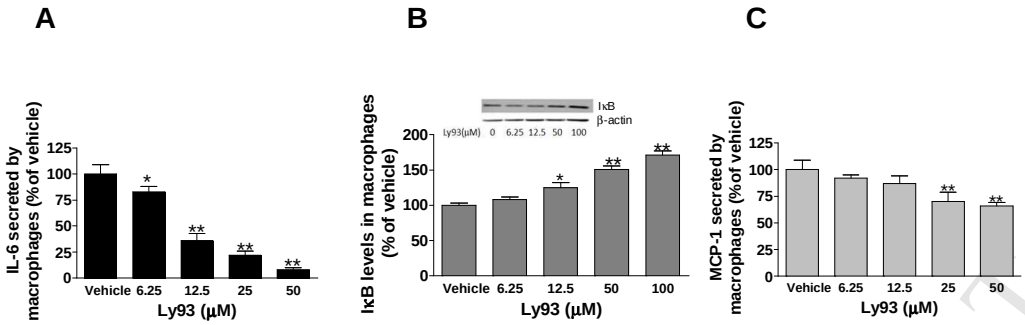

Fig 6. The *in vitro* inhibitory activities of Ly93 against the LPS-mediated pro-inflammatory cytokine and chemokine secretion in macrophages. (A) IL-6 secreted by macrophages in culture medium after LPS (10 ng/ml for 16 h) treatment. (B) Western blot of IκB after LPS treatment (insert) and the quantitation was displayed. (C) MCP-1 production in macrophages induced by LPS. Values are mean ± SD, $n = 7$. *$P < 0.05$, **$P < 0.01$.

2.9 The pharmacokinetics of Ly93.

Studies on the pharmacokinetics of Ly93 were performed on C57BL/6J mice according to the procedures shown in the part of **Materials and Methods**. The representative mass spectra and chromatograms of Ly93 in plasma were shown in **Supplementary Fig. 3**. The plasma concentration-time profiles of different Ly93 doses were shown in **Fig. 7A**. The pharmacokinetic parameters of Ly93 after intragastric administration in C57BL/6J mice were shown in **Supplementary Table 2**. The $AUC_{0\sim8h}$ could amount to 6.26 μg·h/ml and the maximum concentration (C_{max}) could reach 6.12 μg/ml when mice were treated by the intragastric administration with a single dose of Ly93 (50 mg/kg). Moreover, as shown in **Fig. 7B**, the $AUC_{0\text{-}8h}$ were linearly correlated with the intragastric administration doses of Ly93 (R^2 = 0.989). The high *Vz*/*F* indicated that compound Ly93 was with good permeability. The pharmacokinetic results demonstrated that compound Ly93 with reasonable physicochemical properties was suitable for the further *in vivo* evaluations.

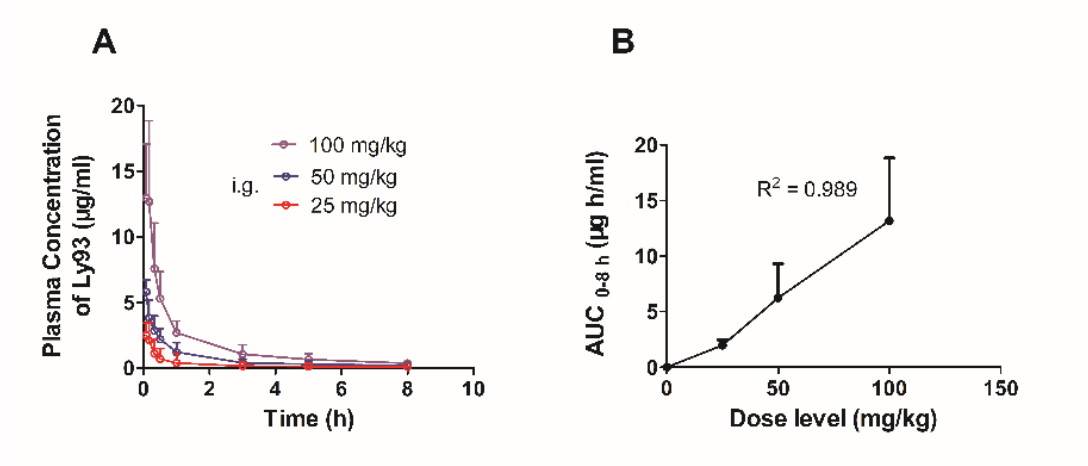

Fig 7. The pharmacokinetics of Ly93. (A) Plasma concentration-time profile of Ly93. (B) The correlation between Ly93 $AUC_{0\text{-}8h}$ and dose from 25 to 100 mg/kg after i.g. administration. Values are mean ± SD, n = 6.

2.10 The effects of Ly93 on plasma SM levels and liver enzymes in C57BL/6J mice in vivo.

SM levels in the circulation are closely associated with lipoprotein metabolism and the development of atherosclerosis [2, 7]. In order to investigate the impact of Ly93 on the plasma SM level *in vivo*, C57BL/6J mice were treated with Ly93 (100 mg/kg, i.g.) once daily for 7 days. The plasma SM levels were analyzed at day 0, 3 and 7. As shown in **Fig. 8A**, the treatment of Ly93 significantly decreased the plasma SM levels compared with vehicle group. At day 7, the concentration of Ly93 in livers were also determined and compared with the concentration of Ly93 in blood. It was found that the Ly93 concentrations in livers were five-fold higher than that in plasma (**Fig. 8B**). The enriched concentration of Ly93 in the liver would favor the inhibition of SMS activities and the attenuation of SM in plasma *in vivo*. Moreover, the concentration of plasma alanine aminotransferase (ALT) and aspartate aminotransferase (AST) in C57BL/6J mice at day 7 were determined to investigate the impact of Ly93 on the liver enzymes. As shown in **Fig. 8C**, the concentration of plasma ALT and AST in Ly93-treated C57BL/6J mice did not exhibit significant changes in the mice of the vehicle group. As the obvious reduction of SM level in plasma was observed on Ly93-treated C57BL/6J mice, Ly93 as a selective SMS2

inhibitor was investigated for its atherosclerotic activities on the animal model.

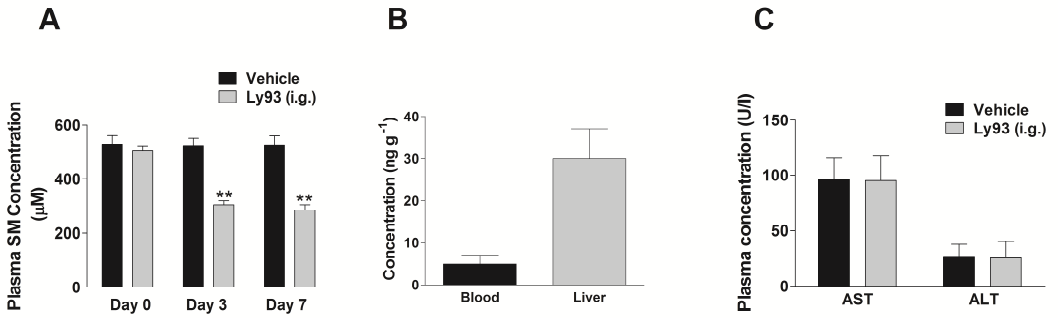

Fig 8. The effects on plasma SM concentration and liver enzymes by the treatment of Ly93 *in vivo*. (A) Plasma SM levels at day 0, 3 and 7 after Ly93 (i.g., 100 mg/kg) treatment once daily for 7 days (n = 10). (B) Ly93 distribution in blood and liver measured at day 7 after Ly93 (i.g., 100 mg/kg) treatment once daily for 7 days (n = 5). (C) AST and ALT levels at day 7 after a daily application of Ly93 (i.g., 100 mg/kg) (n = 10). Values are mean ± SD, $^{**}P < 0.01$.

2.11 The in vivo anti-atherosclerotic activities of Ly93 in apoE KO mice.

As it was shown in **Supplementary Fig. 4**, an *in vivo* experiment was designed to investigate the anti-atherosclerotic activities of Ly93 in apoE KO mice which are the acknowledged experimental animal model of spontaneous atherosclerosis. Firstly, thirty apoE KO mice which were eight-week-old had been fed with the Western-type diet for six weeks. Then thirty mice were equally divided into three groups and subsequently had been treated (i.g.) daily with vehicle, low dose (12.5 mg/kg) and high dose (40 mg/kg) of Ly93 respectively along with the Western-type diet for seven weeks.

During the trial, the body weights of all apoE KO mice in three groups were monitored weekly to investigate the effect of Ly93 on the normal growth of apoE KO mice. As it was shown in **Supplementary Fig. 5**, the growth curves of apoE KO mice did not significantly change in either group. At the end of the experiment, the levels of ALT and AST in the plasma of apoE KO mice were tested to investigate the accumulative effect of Ly93 on the animal livers. As it was shown in **Supplementary**

Fig. 6, the levels of ALT and AST in the plasma of apoE KO mice which were treated by Ly93 did not show statistic changes when compared with the control group.

2.11.1 The effects on the liver SMS activities and plasma SM levels of apoE KO mice by Ly93 treatment.

The livers of apoE KO mice were homogenized for the determination of SMS activities. As shown in **Fig. 9A**, liver SMS activities in low dose and high dose groups showed significant reductions (-35% and -39%, respectively; $P < 0.05$). Furthermore, plasma SM levels of Ly93-treated mice were measured. It was found that there was a significant and dose-dependent reduction in the SM levels of Ly93-treated mice as compared with control animals (-25% and -41%, respectively; $P < 0.05$ and $P < 0.01$; **Fig. 9B**).

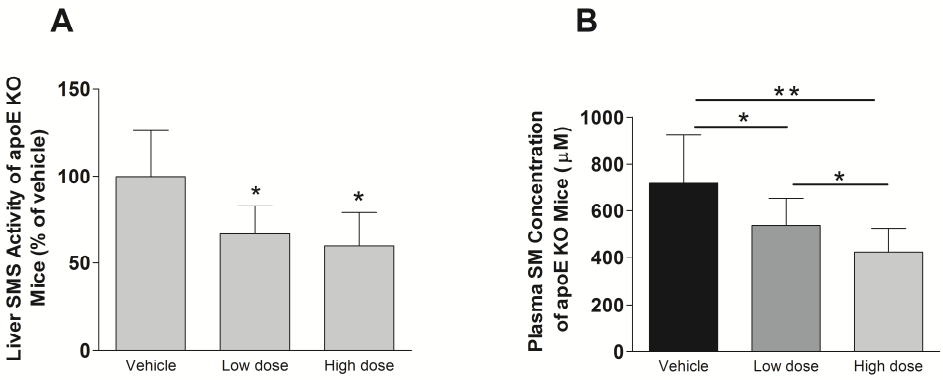

Fig 9. The liver SMS activities and SM levels in Ly93-treated apoE KO mice. (A) SMS activity in apoE KO mice liver after Ly93 treatment. (B) Plasma SM levels in apoE KO mice after Ly93 treatment. Low dose: 12.5 mg/kg, i.g., High dose: 40 mg/kg, i.g.. Values are mean ± SD, $n = 10$. *$P < 0.05$, **$P < 0.01$.

2.11.2 The blood cell analysis of apoE KO mice by flow cytometry after Ly93 treatment.

SM levels on the plasma membrane of certain blood cells, such as lymphocytes, are closely associated with inflammation and the development of atherosclerosis. Flow

cytometry was utilized to evaluate the effect of Ly93 treatment on blood cells which participate in the process of atherosclerosis. As shown in **Fig. 10A** and **10B**, the lymphocyte in mice of Ly93-low dose group and Ly93-high dose group were lowered by 21% and 24% respectively compared with that of vehicle-treated group. The monocyte (**Fig. 10A** and **10C**) were significantly lowered in Ly93-low dose group (-51%, $P < 0.001$) and Ly93-high dose group (-50%, $P < 0.001$), compared with control group. CD4+/CD8+ cell ratios were reduced in Ly93-low dose group (-34%, $P < 0.01$) and Ly93-high dose group (-37%, $P < 0.01$), compared with vehicle-treated group (**Fig. 10D** and **10E**). Moreover, CD11b+CD11c+ subset of dendritic cells in Ly93-high dose group was dramatically decreased by 57% ($P < 0.05$), while no significant changes were found between Ly93-low dose group and control group (**Fig. 10F** and **10G**). CD11b+Ly6C++ and Ly6G+cells were attenuated by 16% ($P < 0.05$) in Ly93-low dose group and 43% ($P < 0.01$) in Ly93-high dose group compared with vehicle group (**Fig. 10H** and **10I**).

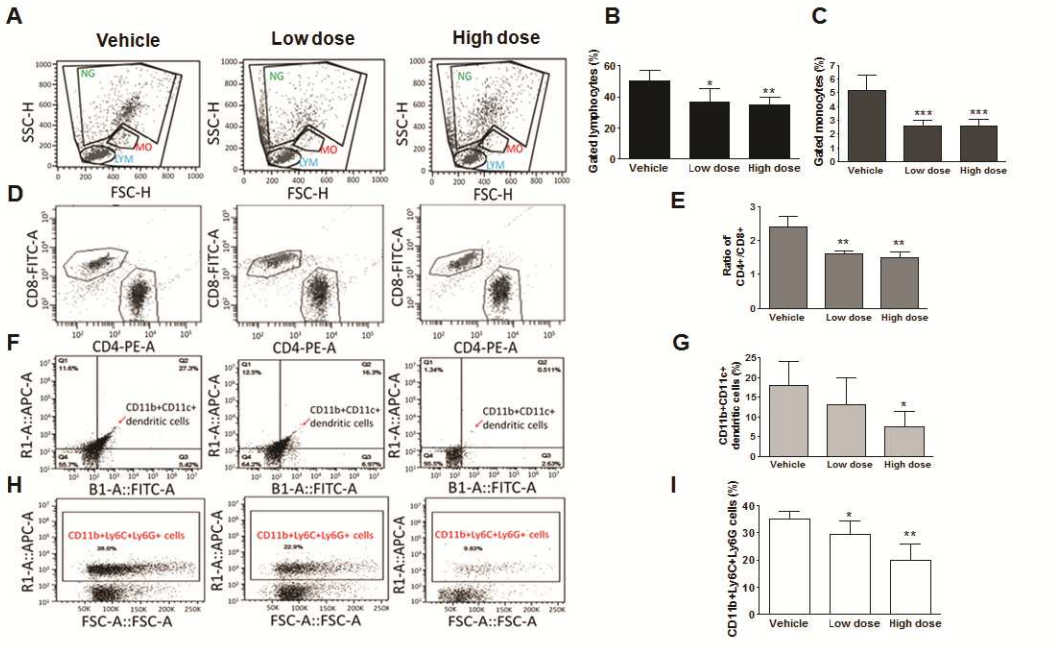

Fig 10. The blood cell analysis by flow cytometry in apoE KO mice after Ly93 treatment. (A) Representatives of the analysis of blood neutrophile granulocytes (NG), lymphocytes and monocytes in vehicle and Ly93 treated animals. (B-C)

Quantitative display of gated lymphocytes and monocytes. (D) Representatives of the analysis of blood CD4+ T cells and CD8+ T cells. (E) Quantitative display of the ratio of CD4+ and CD8+ T cells. (F) Representatives of the analysis of blood CD11b+CD11c+ dendritic cells. (G) Quantitative display of the percentage of the dendritic cells. (H) Representatives of the analysis of blood CD11b+Ly6c+Ly6G+ cells. (I) Quantitative display of CD11b+Ly6c+Ly6G+ cells. Values are mean ± SD, $n = 5$, $^{*}P < 0.05$, $^{**}P < 0.01$, $^{***}P < 0.001$.

2.11.3 The effects on the development of atherosclerosis in apoE KO mice by Ly93 treatment.

ApoE KO mice were sacrificed after 7 weeks of treatment with Ly93. The proximal aortae and aortic arches of mice in each group were dissected and photographed. The lesion areas of mice in each group were measured to evaluate the inhibitive effect of Ly93 on atherogenesis. Aortic arches with atherosclerotic plaques were shown in **Fig. 11A**. All mice were found present lesions in aortic arches. However, those of Ly93 groups were noticeably smaller than those of vehicle-treated group. In addition, significantly reduced lesion areas in Ly93-low dose group and Ly93-high dose group were revealed by oil-red O in the whole aorta of apoE KO mice (-32% and -41%, respectively; $P < 0.05$ and $P < 0.01$; **Fig. 11B** and **11C**). Furthermore, there were dose-dependently decreased lesions between two Ly93-treated groups. The proximal aorta of mice in Ly93 groups also showed decreased lesion areas by hematoxylin and eosin (H&E) staining compared with animals in vehicle-treated group (-38% and -50%, respectively; $P < 0.01$; **Fig. 11D** and **11E**). Immunostaining was then performed to determine macrophage accumulation and investigated the affection of Ly93 treatment on the composition of lesions in the aortic root of apoE KO mice. Although all sections stained positively for monocyte/macrophage markers (MOMA), mice in Ly93-treated groups had a significant reduction in macrophage content compared with that in vehicle-treated group (-28% and -55%, respectively; $P < 0.05$ and $P < 0.01$; **Fig. 11F**

and **11G**).

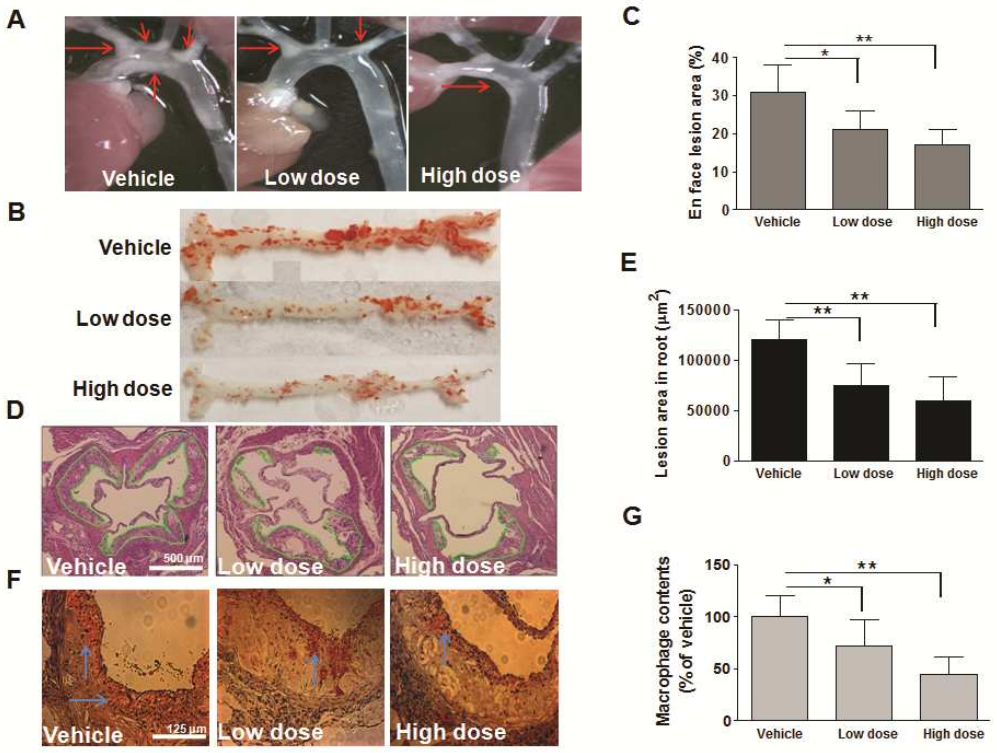

Fig 11. The effects on the development of atherosclerosis in apoE KO mice with Ly93 treatment. 8-week-old apoE KO mice were fed with a high fat and cholesterol diet for 6 weeks, and then the mice in three groups were treated with vehicle (i.g.), low dose Ly93 (12.5 mg/kg, i.g.) and high dose Ly93 (40 mg/kg, i.g.) respectively every day for 7 weeks. (A) Aortic arches with atherosclerotic plaques (red arrows). (B) *Enface* aortic plaque analysis after Oil Red O staining. (C) Quantitative display of *en faces* aortic plaque. (D) Aortic root assay for lesion areas after Hematoxylin and eosin staining. (E) Quantitative display of lesion areas in the aortic root. (F) Immunohistochemical staining of macrophage accumulation in lesions (shown as brown stained regions indicated by blue arrows). (G) Quantitative display of macrophage content. Quantifications were done by using Image J software. Six alternate sections (4 μm thick) sliced from paraffin-fixed aortic root tissues of each transplanted mouse were used for the analysis. Values are mean ± SD. $n = 9$, $^{*}P < 0.05$, $^{**}P < 0.01$.

3. Discussion and Conclusion

In this study, the 2-benzyloxybenzamide (D2-e) was firstly discovered as SMS2 inhibitor through scaffold hopping of lead compound D2. D2-e was tested with moderate SMS2 inhibitory activity (IC_{50} = 13.4 μM). Then, a series of 2-benzyloxybenzamides were designed and synthesized through structural optimization. The newly obtained compounds were put into the evaluation of the SMS2 inhibitory activities. The results of *in vitro* enzymatic assays revealed that the optimized compounds had significantly improved the SMS2 inhibitory activities compared with D2-e. The structure-activity relationships were also studied based on the *in vitro* enzymatic inhibitory activities. The 2-benzyloxybenzamides were proved to be with more potential toward SMS2 inhibition and higher selectivity over SMS1 than the oxazolopyridine derivatives obtained from the lead compound D2 [31]. Furthermore, the 2-benzyloxybenzamide compound **10** with improved inhibitory activity toward purified SMS2 (IC_{50} = 1.5 μM) became an optimal lead compound that promoted the discovery of 4-benzyloxybenzo[*d*]isoxazole-3-amine derivatives as selective SMS2 inhibitors [33].

Among the 2-benzyloxybenzamides, the novel small molecule Ly93 was one of the most potent SMS2 inhibitors. Considering its prominent SMS2 inhibitory activity and optimal properties, Ly93 was selected for further studies. Fortunately, it exhibited nanomolar inhibitory activity against purified SMS2 (IC_{50} = 91 nM). The selectivity ratio of Ly93 was more than 1400-fold for purified SMS2 over SMS1 (IC_{50} = 133.9 μM). The binding modes of Ly93 with the homology model of *h*SMS2 were predicted by the molecular docking study. It demonstrated that Ly93 bound with *h*SMS2 at the same active site as other reported SMS2 inhibitors [28, 31, 33]. Therefore, Ly93, as a novel selective SMS2 inhibitor, was utilized as a validation tool for the investigations of SMS2-relevant pathways.

In Huh7 cells, the treatment of Ly93 decreased the apoB secretion from

hepatocytes in a dose-dependent manner. It was in accordance with the previous studies that SM has significant effects on the metabolism of atherogenic lipoproteins [1]. In macrophages, Ly93 attenuated the intracellular SMS activity and simultaneously increased the cholesterol efflux that involves in the reverse cholesterol transport and anti-atherogenic process. Moreover, due to the decreased SM in the macrophage membrane, Ly93 depressed the secretion of LPS-mediated pro-inflammatory cytokine and chemokine from macrophages indirectly. Since it has been reported that cellular SM in macrophage is one of the major factors that modulate the atherogenic functions of macrophage [12], it is conceivable that SMS inhibition-mediated membrane SM reduction could have consequences in terms of macrophage inflammation and cholesterol efflux which are the critical factors of atherogenesis. The effects of Ly93 on the cholesterol efflux and inflammatory responses in macrophages could further contribute to the anti-atherosclerotic activities *in vivo*.

Considering the linear correlation of $AUC_{0\text{-}8h}$ between doses of Ly93 after intragastric administration, Ly93 was further studied the SMS inhibitory activities *in vivo*. Ly93 induced the inhibition of SMS that specifically reduced the plasma SM levels in C57BL/6J mice without obvious effects on the liver enzymes. This could make contributions to the reduction of atherosclerosis mediated by SM-enriched lipoproteins.

Since the reduction of plasma SM levels was observed in Ly93-treated C57BL/6J mice, the further *in vivo* studies were conducted in apoE KO mice that are an acknowledged model of spontaneous atherosclerosis. The 7-week treatment of Ly93 significantly decreased the SMS activities in mice livers and SM levels in plasma in a dose-dependent manner. However, the levels of cholesterol and triglyceride in apoE KO mice were not significantly impacted by the treatment of Ly93 (**Supplementary Fig. 7**). It was indicated that the selective inhibition of SMS2 could specifically reduce the SM level.

In previous studies, it has been reported that SM levels on the plasma membrane of lymphocytes and monocytes are closely associated with inflammation and the development of atherosclerosis [39, 40]. In this study, the SMS inhibition with the treatment of Ly93 could reduce the lymphocytes and monocytes in apoE KO mice indicating the decreased inflammatory responses and atherosclerosis. It was also demonstrated that inhibition of SMS activity could raise the ratio of CD8+T/CD4+T. The results were in accordance with the reported studies that a subset of CD8+T cells could reduce atherosclerotic lesions in apoE KO mice [41].

In the process of atherosclerosis development, CD11b+CD11c+ subset of dendritic cells was rapidly increased [42-44]. Dendritic cells in the aorta intimal rapidly ingest lipid and become foam cells when mice were fed with high fat/high cholesterol diet. Depletion of these intimal dendritic cells reduces foam cell formation [43]. Deficiency of CD11c+, a surface marker on dendritic cells, reduced atherosclerotic lesions [44]. Our result indicated that SMS inhibition reduces CD11b+CD11c+ dendritic cells in the blood (**Fig. 10F** and **10G**). This could contribute to the reduction of atherosclerosis in apoE KO mice. CD11b+Ly6C+ and Ly6G+ cells (granulocytic myeloid-derived suppressor cells, granulocytic MDSCs) are also involved in pro-inflammatory processes and chronic inflammation [45, 46]. These cells were reduced by Ly93 treatment in a dose-dependent manner (**Fig. 10H** and **10I**). The significance of these changes, as related to atherosclerosis, deserves further studies.

Finally, the body weights and liver enzymes of Ly93-treated apoE KO mice did not exhibit significant changes with those of vehicle group. It could suggest that the Ly93 scarcely induce side-effects on the apoE KO mice. Under the safe treatment of Ly93 for 7 weeks, the selective SMS2 inhibitor attenuated the atherosclerotic plaque in aortic arches and root as well as in the entire aorta. Meanwhile, the accumulation of macrophages in atherosclerotic lesions was prevented by Ly93. As macrophages participate in the atherogenic processes including inflammatory responses and the

formation of foam cells, the reduced macrophages in atherosclerotic lesions could suggest that Ly93 directly impact the macrophages through which it indirectly prevents the development of atherosclerosis.

In summary, 2-benzyloxybenzamides were discovered as novel SMS2 inhibitors. Ly93 was found to be a novel orally efficacious selective SMS2 inhibitor with nanomolar SMS2 inhibitory activity. In *in vivo* studies, Ly93 dose-dependently inhibited the liver SMS activities, reduced the plasma SM levels and finally attenuated the development of atherosclerosis. The results of *in vitro* assays demonstrated that Ly93 diminished apoB secretion from Huh7 cells, reduced the SMS activity and increased cholesterol efflux in macrophages in a dose-dependent manner. Meanwhile, Ly93 could inhibit the secretion of LPS-mediated pro-inflammatory cytokine and chemokine in macrophages. These preliminary molecular mechanism-of-action studies showed that Ly93 could affect both lipid homeostasis and inflammation process. To our knowledge, it is the first study that selective SMS2 inhibitor is investigated the anti-atherosclerotic activities *in vivo*, which would make contributions to the further studies on the SMS2-relevant pathways and promote the development of selective SMS2 inhibitor to be a promising treatment for atherosclerosis.

4. Materials and Methods

4.1 Materials

Reagents used in the chemical synthesis were purchased from commercial sources and were used without further purification except for the special case. Flash column chromatography was carried out at medium pressure using silica gel (200-300 mesh) purchased from Qingdao Haiyang Chemical Co. Ltd. All the reactions were monitored by thin layer chromatography (TLC) on silica gel. Mass spectra data were given with electrospray ionization (ESI) produced by a Finnigan MAT-95, LCQ-DECA spectrometer and IonSpec 4.7 T. MS. High-resolution mass spectra data

were given by AB 5600+ Q TOF. ^{1}HNMR and ^{13}CNMR spectra data were obtained on Varian Mercury Plus 400 spectrometers working at 400 MHz or Bruker Ascend™ 600 spectrometers working at 600 MHz. Chemical shifts (δ) were reported in parts per million (ppm) relative to internal tetramethylsilane (TMS) and *J* values were reported in Hertz. Peak multiplicity was described as singlet (s), doublet (d), triplet (t), quartet (q), multiplet (m), double doublet (dd), double triplet (dt), double-double doublet (ddd), triple doublet (td). The purities of all tested 2-benzyloxybenzamides were higher than 95% by HPLC, which were performed on an Agilent 1260 HPLC system (Agilent Technologies, Palo Alto, CA, USA) with a G1311B quaternary pump, a G1329B ALS and a G4212B DAD detector. An Agilent C18 RP column (250 mm × 4.6 mm, 5 μm) was employed in the chromatographic separations. The HPLC method consisted of the following: column temperature 25 ^{o}C; inject volume 20 μl; HPLC solvent H_2O (0.1% formic acid)/methanol = 25/75 (v/v); flow rate of 1.0 ml/min; detector wavelength of 254 nm. Melting points were determined by an SGW X-4 thermometer and were uncorrected (slide method). The yield was not optimized.

6-((*N*-(7-nitrobenz-2-oxa-1,3-diazol-4-yl)amino)hexanoyl)-sphingosine (C6-NBD-Cer) and 1,2-dimyristoyl-*sn*-glycero-3-phosphocholine (DMPC) were purchased from Santa Cruz Inc (USA). Milli-Q deionized water from a Millipore water purification system (Bedford, MA, USA) was used throughout the study. All other reagents were of analytical grade. Dulbecco's modified Eagle's medium (DMEM) and fetal bovine serum (FBS) were purchased from Thermo Scientific HyClone, Shiyi Biotechnology, Shanghai, China. L-[^{35}S]-methionine (specific activity 1175 Ci/mmol) and Cholesterol, [1, 2-^{3}H(N)] (49.0 Ci/mmol) were purchased from Perkin Elmer, Boston, MA. Chromatographically purified LPS from S. Minnesota was purchased from Sigma-Aldrich, St. Louis, MO. IκBα Rabbit antibody was purchased from Abcam (ab32518). Male (C57BL/6J) mice aged 8 weeks were purchased from the Animal Center of the School of Pharmacy, Fudan University, Shanghai, China. All animal experiments were approved by the Animal

Care and Use Committee of the University of Fudan and were in accordance with the National Institutes of Health guidelines.

4.2 Chemistry

All intermediate compounds' experimental conditions and their data for structure elucidation were collected in the **Supplementary Material**.

4.2.1 General procedure for the preparation of 6, 7, 9 and 10

A mixture of **4a** (0.55 g, 2.4 mmol) in thionyl chloride (7.3 ml) and catalytic pyridine (0.04 ml) was stirred and refluxed for 2.5 h. After cooling to ambient temperature, the thionyl chloride was evaporated and the crude product 2-(benzyloxy)benzoyl chloride was obtained as light yellow solid.

A mixture of amines **5** (2 mmol) in dichloromethane (10 ml) and pyridine (0.32 ml, 4 mmol) was added the solution of 2-(benzyloxy)benzoyl chloride (2 mmol) in dichloromethane (10 ml) slowly at 0 ^{o}C. The reaction mixture was stirred at room temperature for 2.0 h, washed with water and brine, dried over Na_2SO_4. After the organic solvent was evaporated, the crude product was purified by flash chromatograph eluting with ethyl acetate/petroleum ether (1:2, *v*: *v*) to afford **6**, **7**, **9** and **10**.

4.2.2 N-benzyl-2-(benzyloxy)benzamide (6)

The title compound was obtained starting from **4a** and benzylamine **5a** (0.21 g, 2 mmol) according to the general procedure. 0.33 g white solid **6**, yield 52.4%, m.p 73.4-75.5^{o}C. ESI-MS(*m/z*): 318.2$[M+H]^+$. HRMS (ESI) of $C_{21}H_{19}NO_2$ $[M+H]^+$ calcd, 318.1489; found, 318.1496. ^{1}H NMR (400 MHz, DMSO-d_6) δ 8.65 (t, J = 5.8 Hz, 1H), 7.69 (dd, J = 7.6, 1.8 Hz, 1H), 7.47 – 7.38 (m, 3H), 7.36 – 7.28 (m, 3H), 7.24 – 7.17 (m, 6H), 7.02 (t, 1H), 5.21 (s, 2H), 4.43 (d, J = 6.0 Hz, 2H). ^{13}C NMR (101 MHz, DMSO-d_6) δ 165.33, 155.76, 139.19, 136.43, 131.90, 130.17, 128.46, 128.24,

127.96, 127.73, 127.10, 126.66, 124.03, 120.74, 113.31, 69.91, 42.59. HPLC purity: 98.9%.

4.2.3 2-(benzyloxy)-N-(furan-2-ylmethyl)benzamide (7)

The title compound was obtained starting from **4a** and furan-2-ylmethanamine **5b** (0.19 g, 2 mmol) according to the general procedure. 0.17 g white solid **7**, yield 27.9%, m.p 45.1-47.2°C. ESI-MS(*m/z*): 308.1$[M+H]^+$. HRMS (ESI) of $C_{19}H_{17}NO_3$ $[M+H]^+$ calcd, 308.1281; found, 308.1284. ^{1}H NMR (400 MHz, DMSO-d_6) δ 8.56 (s, 1H), 7.72 (d, J = 7.3 Hz, 1H), 7.52 (s, 1H), 7.43 (dd, J = 14.1, 7.3 Hz, 3H), 7.34 (dd, J = 15.1, 7.4 Hz, 3H), 7.21 (d, J = 8.3 Hz, 1H), 7.03 (t, J = 7.4 Hz, 1H), 6.33 (s, 1H), 6.13 (s, 1H), 5.21 (s, 2H), 4.43 (d, J = 5.5 Hz, 2H). ^{13}C NMR (101 MHz, DMSO-d_6) δ 165.02, 155.84, 151.93, 142.09, 136.35, 132.18, 130.35, 128.51, 127.95, 127.62, 123.37, 120.80, 113.40, 110.44, 106.77, 69.96, 36.05. HPLC purity: 98.5%.

4.2.4 2-(benzyloxy)-N-(pyridin-2-yl)benzamide (9)

The title compound was obtained starting from **4a** and pyridin-2-amine **5d** (0.19 g, 2 mmol) according to the general procedure. 0.36 g white solid **9**, yield 60.0%, m.p 112.3-114.9°C. ESI-MS(*m/z*): 305.2$[M+H]^+$. HRMS (ESI) of $C_{19}H_{16}N_2O_2$ $[M+H]^+$ calcd, 305.1285, found 305.1291. ^{1}H NMR (400 MHz, DMSO-d_6) δ 10.58 (s, 1H), 8.30 (dd, J = 4.8, 1.0 Hz, 1H), 8.22 (d, J = 8.3 Hz, 1H), 7.86 (dd, J = 7.7, 1.7 Hz, 1H), 7.84 – 7.77 (m, 1H), 7.53 (dd, J = 13.9, 4.5 Hz, 3H), 7.39 – 7.28 (m, 4H), 7.12 (dt, J = 12.3, 4.1 Hz, 2H), 5.34 (s, 2H). ^{13}C NMR (101 MHz, DMSO-d_6) δ 163.93, 156.04, 151.56, 148.19, 138.33, 136.10, 133.18, 130.76, 128.45, 128.03, 127.72, 122.83, 121.15, 119.80, 113.75, 70.35. HPLC purity: 99.0%.

4.2.5 2-(benzyloxy)-N-(pyridin-3-yl)benzamide (10)

The title compound was obtained starting from **4a** and pyridin-3-amine **5e** (0.19

g, 2 mmol) according to the general procedure. 0.28 g white solid **10**, yield 46.7%, m.p 107.6-108.9°C. ESI-MS(*m/z*): 305.2$[M+H]^+$. HRMS (ESI) of $C_{19}H_{16}N_2O_2$ $[M+H]^+$ calcd, 305.1285, found 305.1288. ^{1}H NMR (400 MHz, DMSO-d_6) δ 10.36 (s, 1H), 8.68 (d, J = 2.3 Hz, 1H), 8.27 (dd, J = 4.7, 1.3 Hz, 1H), 8.10 (d, J = 8.3 Hz, 1H), 7.69 (dd, J = 7.6, 1.6 Hz, 1H), 7.57 – 7.50 (m, 3H), 7.40 – 7.32 (m, 4H), 7.30 (d, J = 8.3 Hz, 1H), 7.11 (t, J = 7.4 Hz, 1H), 5.25 (s, 2H). ^{13}C NMR (101 MHz, DMSO-d_6) δ 165.40, 156.16, 144.85, 141.33, 136.98, 136.07, 132.89, 130.34, 129.30 – 128.03, 126.73, 125.07, 124.15, 121.39, 113.84, 70.59. HPLC purity: 98.4%.

4.2.6 General procedure for the preparation of 8 and 11

To a solution of **4a** or **4b** (3 mmol) in dried dichloromethane (15 ml) was added EDCI (0.86 g, 4.5 mmol) and DMAP (0.04 g, 0.3 mmol) at 0 °C. After the amine **5c** or **5f** (3 mmol) was added into the mixture, the reaction was stirred at room temperature for 2.0 h. Then the mixture was extracted with ethyl acetate, washed with brine and dried over Na_2SO_4. After the organic solvent was evaporated, the crude product was purified by flash chromatograph eluting with ethyl acetate/petroleum ether to afford **8** and **11**.

4.2.7 2-(benzyloxy)-N-cyclohexylbenzamide (8)

The title compound was obtained starting from **4a** and cyclohexanamine **5c** according to the general procedure. The crude product was purified by flash chromatograph eluting with ethyl acetate/petroleum ether (1:20, *v*: *v*) to afford **8**. White solid, yield 36.6%, m.p 54.2-55.6°C. ESI-MS(*m/z*): 310.1$[M+H]^+$. HRMS (ESI) of $C_{20}H_{23}NO_2$ $[M+H]^+$ calcd, 310.1802, found 310.1806. ^{1}H NMR (400 MHz, DMSO-d_6) δ 7.98 (d, J = 7.8 Hz, 1H), 7.75 (dd, J = 7.7, 1.8 Hz, 1H), 7.54 – 7.49 (m, 2H), 7.49 – 7.33 (m, 4H), 7.24 (d, J = 8.2 Hz, 1H), 7.07 – 7.00 (m, 1H), 5.17 (s, 2H), 3.77 – 3.63 (m, 1H), 1.71 – 1.60 (m, 2H), 1.43 (d, J = 9.2 Hz, 3H), 1.26 – 1.11 (m,

2H), 1.09 – 0.93 (m, 3H). ^{13}C NMR (151 MHz, DMSO-d_6) δ 163.74, 156.13, 136.18, 132.10, 130.49, 128.52, 128.42, 128.33, 123.30, 120.84, 113.23, 70.49, 47.35, 32.04, 25.22, 23.98. HPLC purity: 99.1%.

4.2.8 2-((2-chlorobenzyl)oxy)-N-(piperidin-3-yl)benzamide (11)

The title compound was obtained starting from **4b** and **5f** according to the general procedure. The crude product was purified by flash chromatograph eluting with ethyl acetate/petroleum ether (1:2, *v*: *v*) to afford **11**. White solid, yield 67.8%, m.p 218.3-222.2^{o}C. ESI-MS(*m/z*): 345.1[M+H]$^{+}$. HRMS (ESI) of $C_{19}H_{21}ClN_2O_2$ [M+H]$^{+}$ calcd, 345.1364, found 345.1362. ^{1}H NMR (400 MHz, DMSO-d_6) δ 9.16 (d, *J* = 55.6 Hz, 2H), 8.18 (d, *J* = 7.5 Hz, 1H), 7.70 – 7.64 (m, 1H), 7.61 (dd, *J* = 7.6, 1.4 Hz, 1H), 7.56 – 7.51 (m, 1H), 7.51 – 7.44 (m, 1H), 7.44 – 7.37 (m, 2H), 7.24 (d, *J* = 8.3 Hz, 1H), 7.05 (t, *J* = 7.4 Hz, 1H), 5.25 (s, 2H), 4.17 – 4.06 (m, 1H), 3.22 (d, *J* = 10.4 Hz, 1H), 3.09 (d, *J* = 12.4 Hz, 1H), 2.66 (d, *J* = 32.8 Hz, 2H), 1.83 – 1.54 (m, 3H), 1.30 (dd, *J* = 19.7, 10.6 Hz, 1H). ^{13}C NMR (101 MHz, DMSO-d_6) δ 165.11, 155.45, 133.90, 132.32, 132.06, 130.19, 130.06, 129.97, 129.41, 127.45, 124.24, 121.01, 113.25, 67.53, 45.97, 43.18, 42.69, 27.81, 20.35. HPLC purity: 98.2%.

4.2.9 2-hydroxy-N-(pyridin-3-yl)benzamide (12)

To a solution of **10** (5.01 g, 16.46 mmol) in methanol (85 ml) was added 10% Pd/C (0.25 g). The reaction mixture was stirred at 3 atmosphere of hydrogen and room temperature for 2.0 h. After the catalytic Pd/C was filtrated, the filtrate was condensed and **12** was obtained as white solid (3.47 g, yield 98.6%). ESI-MS(*m/z*): 215.1[M+H]$^{+}$. ^{1}H NMR (400 MHz, DMSO-d_6) δ 11.65 (s, 1H), 10.53 (s, 1H), 8.88 (d, *J* = 2.4 Hz, 1H), 8.35 (dd, *J* = 4.7, 1.4 Hz, 1H), 8.17 (ddd, *J* = 8.3, 2.4, 1.5 Hz, 1H), 7.95 (dd, *J* = 7.9, 1.6 Hz, 1H), 7.49-7.39 (m, 2H), 7.04-6.95 (m, 2H).

4.2.10 General procedure for the preparation of 19-21, 24-28, 31 and 32

To a solution of **12** (0.21 g, 1.0 mmol) in acetone (6 ml) was added various commercially avaliable benzyl bromides **18a-18j** (1.0 mmol) and K_2CO_3 (0.28 g, 2.0 mmol). The reaction mixture was stirred at room temperature for 1.0 h and then evaporated the solvent. The residue was extracted with ethyl acetate, washed with brine and dried over Na_2SO_4. After the organic solvent was evaporated, the crude product was purified by flash chromatograph eluting with ethyl acetate/petroleum ether (1:2, *v*: *v*) to afford **19-21**, **24-28**, **31** and **32**.

4.2.11 2-((2-fluorobenzyl)oxy)-N-(pyridin-3-yl)benzamide (19)

The title compound was obtained starting from **12** and **18b** according to the general procedure. White solid **19**, yield 71.9%, m.p 101.6-102.5^{o}C. ESI-MS(*m/z*):323.2$[M+H]^+$. HRMS (ESI) of $C_{19}H_{15}FN_2O_2$ $[M+H]^+$ calcd, 323.1190, found 323.1194. ^{1}H NMR (400 MHz, DMSO-d_6) δ 10.56 (s, 1H), 8.86 (d, J = 1.8 Hz, 1H), 8.39 (dd, J = 4.9, 1.1 Hz, 1H), 8.22 (d, J = 8.4 Hz, 1H), 7.68 (dd, J = 7.6, 1.7 Hz, 1H), 7.66 – 7.61 (m, 1H), 7.60 – 7.53 (m, 2H), 7.44 – 7.34 (m, 2H), 7.25 (dd, J = 9.8, 8.9 Hz, 1H), 7.19 (td, J = 7.5, 0.8 Hz, 1H), 7.14 (t, J = 7.5 Hz, 1H), 5.33 (s, 2H). ^{13}C NMR (101 MHz, DMSO-d_6) δ 165.57, 161.82, 159.37, 155.91, 142.66, 138.80, 136.87, 132.99, 130.97, 130.71, 130.30, 129.07, 125.23, 125.00, 123.97, 123.83, 121.65, 115.98, 115.77, 114.03, 64.75. HPLC purity: 99.1%.

4.2.12 2-((2-chlorobenzyl)oxy)-N-(pyridin-3-yl)benzamide (20)

The title compound was obtained starting from **12** and **18c** according to the general procedure. White solid **20**, yield 75.4%, m.p 96.0-96.2^{o}C. ESI-MS(*m/z*):339.2$[M+H]^+$. HRMS (ESI) of $C_{19}H_{15}ClN_2O_2$ $[M+H]^+$ calcd, 339.0895, found 339.0908. ^{1}H NMR (400 MHz, DMSO-d_6) δ 10.34 (s, 1H), 8.67 (d, J = 2.4 Hz, 1H), 8.28 (dd, J = 4.7, 1.4 Hz, 1H), 8.13 – 8.07 (m, 1H), 7.69 (td, J = 7.7, 1.5 Hz,

2H), 7.54 (ddd, *J* = 9.1, 8.3, 1.3 Hz, 2H), 7.42 – 7.29 (m, 4H), 7.14 (t, *J* = 7.5 Hz, 1H), 5.34 (s, 2H). ^{13}C NMR (101 MHz, DMSO-d_6) δ 165.34, 155.84, 144.90, 141.40, 136.08, 134.41, 132.86, 132.75, 130.41, 130.34, 129.87, 127.82, 126.68, 125.43, 124.12, 121.70, 113.94, 68.08. HPLC purity: 99.3%.

4.2.13 2-((2-methylbenzyl)oxy)-N-(pyridin-3-yl)benzamide (21)

The title compound was obtained starting from **12** and **18d** according to the general procedure. White solid **21**, yield 46.9%, m.p 95.9-98.0^{o}C. ESI-MS(*m/z*):319.2[M+H]$^+$. HRMS (ESI) of $C_{20}H_{18}N_2O_2$ [M+H]$^+$ calcd, 319.1441, found 319.1440. ^{1}H NMR (400 MHz, DMSO-d_6) δ 10.37 (s, 1H), 8.61 (d, *J* = 2.4 Hz, 1H), 8.27 (dd, *J* = 4.7, 1.4 Hz, 1H), 8.09 – 8.02 (m, 1H), 7.69 (dd, *J* = 7.6, 1.7 Hz, 1H), 7.58 – 7.52 (m, 1H), 7.50 (d, *J* = 7.5 Hz, 1H), 7.39 – 7.32 (m, 2H), 7.28 – 7.21 (m, 2H), 7.15 (ddd, *J* = 17.3, 11.2, 4.7 Hz, 2H), 5.26 (s, 2H), 2.34 (s, 3H). ^{13}C NMR (101 MHz, DMSO-d_6) δ 165.44, 156.18, 144.86, 141.32, 136.97, 136.09, 134.95, 132.73, 130.65, 130.17, 128.88, 126.42, 125.33, 124.10, 121.34, 113.96, 69.11, 18.88. HPLC purity: 98.6%.

4.2.14 2-((2-cyanobenzyl)oxy)-N-(pyridin-3-yl)benzamide (24)

The title compound was obtained starting from **12** and **18e** according to the general procedure. White solid **24**, yield 30.4%, m.p 122.8-125.2^{o}C. ESI-MS(*m/z*):330.1[M+H]$^+$. HRMS (ESI) of $C_{20}H_{15}N_3O_2$ [M+H]$^+$ calcd, 330.1237, found, 330.1247. ^{1}H NMR (400 MHz, DMSO-d_6) δ 10.32 (s, 1H), 8.67 (s, 1H), 8.25 (d, *J* = 4.2 Hz, 1H), 8.08 (d, *J* = 8.3 Hz, 1H), 7.88 (d, *J* = 7.6 Hz, 1H), 7.78 (t, *J* = 10.8 Hz, 1H), 7.67 (dd, *J* = 12.1, 7.0 Hz, 2H), 7.53 (dd, *J* = 9.0, 4.4 Hz, 2H), 7.33 (dd, *J* = 12.6, 6.5 Hz, 2H), 7.13 (t, *J* = 7.4 Hz, 1H), 5.41 (s, 2H). ^{13}C NMR (101 MHz, DMSO-d_6) δ 164.89, 155.15, 144.32, 140.93, 139.73, 135.66, 133.42, 133.14, 132.31, 129.85, 129.19, 129.08, 126.36, 125.23, 123.66, 121.35, 117.07, 113.42,

110.76, 68.02. HPLC purity: 98.9%.

4.2.15 2-((3-fluorobenzyl)oxy)-N-(pyridin-3-yl)benzamide (25)

The title compound was obtained starting from **12** and **18f** according to the general procedure. White solid **25**, yield 56.3%, m.p 102.8-104.2°C. ESI-MS(*m/z*):323.1[M+H]$^+$. HRMS (ESI) of $C_{19}H_{15}FN_2O_2$ [M+H]$^+$ calcd, 323.1190, found 323.1199. ^{1}H NMR (400 MHz, DMSO-d_6) δ 10.40 (s, 1H), 8.76 (d, J = 2.4 Hz, 1H), 8.29 (dd, J = 4.7, 1.4 Hz, 1H), 8.18 – 8.10 (m, 1H), 7.67 (dd, J = 7.6, 1.6 Hz, 1H), 7.57 – 7.50 (m, 1H), 7.45 – 7.34 (m, 4H), 7.27 (d, J = 8.3 Hz, 1H), 7.19 – 7.09 (m, 2H), 5.27 (s, 2H). ^{13}C NMR (101 MHz, DMSO-d_6) δ 165.56, 163.88, 161.45, 155.83, 144.87, 141.40, 140.04, 136.16, 132.67, 130.91, 130.21, 126.63, 125.66, 124.09, 123.99, 121.46, 115.00, 113.75, 69.59. HPLC purity: 99.4%.

4.2.16 2-((3-chlorobenzyl)oxy)-N-(pyridin-3-yl)benzamide (26)

The title compound was obtained starting from **12** and **18g** according to the general procedure. White solid **26**, yield 64.9%, m.p 125.1-125.6°C. ESI-MS(*m/z*):339.2[M+H]$^+$. HRMS (ESI) of $C_{19}H_{15}ClN_2O_2$ [M+H]$^+$ calcd, 339.0895, found 339.0895. ^{1}H NMR (400 MHz, DMSO-d_6) δ 10.40 (s, 1H), 8.79 (d, J = 2.4 Hz, 1H), 8.29 (dd, J = 4.7, 1.4 Hz, 1H), 8.20 – 8.07 (m, 1H), 7.66 (dd, J = 7.7, 1.6 Hz, 2H), 7.58 – 7.50 (m, 1H), 7.50 – 7.44 (m, 1H), 7.43 – 7.33 (m, 3H), 7.28 (d, J = 8.3 Hz, 1H), 7.12 (t, J = 7.4 Hz, 1H), 5.25 (s, 2H). ^{13}C NMR (101 MHz, DMSO-d_6) δ 165.56, 155.81, 144.86, 141.42, 139.70, 136.14, 133.69, 132.67, 130.76, 130.20, 128.35, 127.88, 126.62, 125.73, 124.10, 121.48, 113.74, 69.51. HPLC purity: 99.0%.

4.2.17 2-((3-cyanobenzyl)oxy)-N-(pyridin-3-yl)benzamide (27)

The title compound was obtained starting from **12** and **18h** according to the general procedure. White solid **27**, yield 81.0%, m.p 150.2-152.6°C.

ESI-MS(*m/z*):330.1[M+H]$^+$. HRMS (ESI) of $C_{20}H_{15}N_3O_2$ [M+H]$^+$ calcd, 330.1237, found 330.1240. ^{1}H NMR (400 MHz, DMSO-d_6) δ 10.41 (s, 1H), 8.80 (s, 1H), 8.27 (d, J = 4.1 Hz, 1H), 8.11 (d, J = 8.2 Hz, 1H), 7.97 (s, 1H), 7.84 (d, J = 7.8 Hz, 1H), 7.77 (d, J = 7.7 Hz, 1H), 7.62 (d, J = 7.4 Hz, 1H), 7.59 – 7.47 (m, 2H), 7.36 (dd, J = 8.1, 4.7 Hz, 1H), 7.24 (d, J = 8.3 Hz, 1H), 7.10 (t, J = 7.4 Hz, 1H), 5.27 (s, 2H). ^{13}C NMR (101 MHz, DMSO-d_6) δ 165.16, 155.15, 144.32, 140.76, 138.44, 135.76, 132.37, 132.16, 131.73, 131.04, 129.69, 126.27, 125.40, 123.76, 121.06, 118.54, 113.21, 111.43, 68.70. HPLC purity: 98.8%.

4.2.18 2-((2-chloro-5-fluorobenzyl)oxy)-N-(pyridin-3-yl)benzamide (28)

The title compound was obtained starting from **12** and **18i** according to the general procedure. White solid **28**, yield 72.2%, m.p 118.0-119.2^{o}C. ESI-MS(*m/z*):357.1[M+H]$^+$. HRMS (ESI) of $C_{19}H_{14}ClFN_2O_2$ [M+H]$^+$ calcd, 357.0801, found 357.0803. ^{1}H NMR (400 MHz, DMSO-d_6) δ 10.41 (s, 1H), 8.76 (d, J = 2.4 Hz, 1H), 8.29 (dd, J = 4.7, 1.4 Hz, 1H), 8.17 – 8.11 (m, 1H), 7.66 (dd, J = 7.5, 1.6 Hz, 1H), 7.59 – 7.48 (m, 3H), 7.38 (dd, J = 8.3, 4.7 Hz, 1H), 7.31 (d, J = 8.3 Hz, 1H), 7.25 (td, J = 8.5, 3.1 Hz, 1H), 7.15 (t, J = 7.4 Hz, 1H), 5.30 (s, 2H). ^{13}C NMR (101 MHz, DMSO-d_6) δ 165.60, 162.55, 160.12, 155.44, 144.92, 141.40, 137.11, 136.14, 132.68, 131.55, 130.15, 127.33, 126.65, 126.01, 124.10, 121.82, 116.79, 113.89, 67.40. HPLC purity: 99.2%.

4.2.19 2-((2,6-dichlorobenzyl)oxy)-N-(pyridin-3-yl)benzamide (31)

The title compound was obtained starting from **12** and **18a** according to the general procedure. Light yellow solid **31**, yield 64.9%, m.p 115.0-116.4 ^{o}C. ESI-MS(*m/z*):373.1[M+H]$^+$. HRMS (ESI) of $C_{19}H_{14}Cl_2N_2O_2$ [M+H]$^+$ calcd, 373.0505, found 373.0506. ^{1}H NMR (400 MHz, DMSO-d_6) δ 10.16 (s, 1H), 8.51 (d, J = 2.4 Hz, 1H), 8.25 (dd, J = 4.7, 1.4 Hz, 1H), 8.05 – 7.98 (m, 1H), 7.71 (dd, J = 7.6, 1.6 Hz,

1H), 7.63 – 7.53 (m, 3H), 7.47 (dd, *J* = 9.0, 7.0 Hz, 2H), 7.33 (dd, *J* = 8.3, 4.7 Hz, 1H), 7.18 (t, *J* = 7.3 Hz, 1H), 5.43 (s, 2H). ^{13}C NMR (101 MHz, DMSO-d_6) δ 165.01, 156.08, 144.87, 141.25, 136.53, 135.96, 132.95, 132.30, 131.69, 130.37, 129.34, 126.61, 125.57, 124.09, 122.17, 114.71, 66.82. HPLC purity: 98.7%.

4.2.20 2-((3-chloro-2-fluorobenzyl)oxy)-N-(pyridin-3-yl)benzamide (32)

The title compound was obtained starting from **12** and **18j** according to the general procedure. Light yellow solid **32**, yield 75.0%, m.p 149.8-150.6^{o}C. ESI-MS(*m/z*):357.1[M+H]$^{+}$. HRMS (ESI) of $C_{19}H_{14}ClFN_2O_2$ [M+H]$^{+}$ calcd, 357.0801, found 357.0806. ^{1}H NMR (400 MHz, DMSO-d_6) δ 10.33 (s, 1H), 8.72 (d, *J* = 2.4 Hz, 1H), 8.28 (dd, *J* = 4.7, 1.4 Hz, 1H), 8.14 – 8.08 (m, 1H), 7.66 (dd, *J* = 7.6, 1.7 Hz, 1H), 7.63 – 7.51 (m, 3H), 7.39 – 7.32 (m, 2H), 7.21 (t, *J* = 7.9 Hz, 1H), 7.14 (t, *J* = 7.5 Hz, 1H), 5.36 (s, 2H). ^{13}C NMR (101 MHz, DMSO-d_6) δ 165.41, 156.95, 155.63, 154.48, 144.89, 141.43, 136.10, 132.71, 130.99, 130.22, 129.44, 126.69, 126.11, 125.88, 125.79, 124.09, 121.76, 120.21, 114.01, 64.60. HPLC purity: 98.1%.

4.2.21 General procedure for the preparation of 22, 29, 30, 33 and 36-45

To a solution of **12** (0.21 g, 1.0 mmol) in acetone (6 ml) was added various benzyl bromides **18k**-**18x** (1.0 mmol), K_2CO_3 (0.28 g, 2.0 mmol) and catalytic KI. The reaction mixture was stirred at room temperature for 1.0 h and then evaporated the solvent. The residue was extracted by ethyl acetate, washed with brine and dried over Na_2SO_4. After the organic solvent was evaporated, the crude product was purified by flash chromatograph eluting with ethyl acetate/petroleum ether (1:2, *v*: *v*) to afford **22**, **29**, **30**, **33** and **36-45**.

4.2.22 2-((2-ethylbenzyl)oxy)-N-(pyridin-3-yl)benzamide (22)

The title compound was obtained starting from **12** and **18m** according to the general procedure. White solid **22**, yield 72.7%, m.p 158.0-161.3°C. ESI-MS(*m/z*):333.2$[M+H]^+$. HRMS (ESI) of $C_{21}H_{20}N_2O_2(M+H)^+$ calcd, 333.1598, found, 333.1608. ^{1}HNMR (400 MHz, DMSO-d_6) δ 11.06 (s, 1H), 9.18 (d, J = 1.6 Hz, 1H), 8.60 (d, J = 5.3 Hz, 1H), 8.44 (d, J = 8.5 Hz, 1H), 7.94 (dd, J = 8.5, 5.4 Hz, 1H), 7.64 (dd, J = 7.6, 1.6 Hz, 1H), 7.61 – 7.55 (m, 1H), 7.49 (d, J = 7.4 Hz, 1H), 7.40 (d, J = 8.3 Hz, 1H), 7.26 (dt, J = 13.9, 6.5 Hz, 2H), 7.19 – 7.10 (m, 2H), 5.27 (s, 2H), 2.68 (q, J = 7.5 Hz, 2H), 1.12 (t, J = 7.5 Hz, 3H). ^{13}C NMR (101 MHz, DMSO-d_6) δ 166.33, 156.20, 142.74, 138.48, 138.20, 134.27, 133.56, 133.13, 130.02, 129.22, 128.84, 127.43, 126.24, 125.02, 121.34, 114.12, 68.67, 25.02, 15.49. HPLC purity: 99.8%.

4.2.23 2-((2-chloro-6-fluorobenzyl)oxy)-N-(pyridin-3-yl)benzamide (29)

The title compound was obtained starting from **12** and **18n** according to the general procedure. White solid **29**, yield 74.0%, m.p 177.3-179.1°C. ESI-MS(*m/z*):357.1$[M+H]^+$. HRMS (ESI) of $C_{19}H_{14}ClFN_2O_2$ $[M+H]^+$ calcd, 357.0801; found, 357.0804. ^{1}H NMR (600 MHz, DMSO-d_6) δ 10.87 (s, 1H), 9.11 (s, 1H), 8.57 (d, J = 4.8 Hz, 1H), 8.38 (s, 1H), 7.90 (s, 1H), 7.66 – 7.58 (m, 2H), 7.50 – 7.44 (m, 2H), 7.36 (d, J = 8.1 Hz, 1H), 7.28 (t, J = 8.9 Hz, 1H), 7.17 (t, J = 7.5 Hz, 1H), 5.33 (s, 2H). ^{13}C NMR (151 MHz, DMSO-d_6) δ 165.94, 162.65, 160.99, 155.92, 135.86, 133.18, 132.38, 130.10, 126.26, 125.64, 122.13, 122.01, 115.37, 115.22, 114.90, 62.80. HPLC purity: 99.5%.

4.2.24 2-((2,5-dichlorobenzyl)oxy)-N-(pyridin-3-yl)benzamide (30)

The title compound was obtained starting from **12** and **18o** according to the general procedure. White solid **30**, yield 73.0%, m.p 185.0-186.9°C. ESI-MS(*m/z*):373.1$[M+H]^+$. HRMS (ESI) of $C_{19}H_{14}Cl_2N_2O_2$ $[M+H]^+$ calcd,

373.0505, found 373.0513. ^{1}H NMR (600 MHz, DMSO-d_6) δ 11.13 (s, 1H), 9.26 (s, 1H), 8.65 – 8.48 (m, 2H), 7.94 (d, J = 4.7 Hz, 1H), 7.70 – 7.63 (m, 2H), 7.62 – 7.56 (m, 1H), 7.53 (d, J = 8.5 Hz, 1H), 7.42 (dd, J = 8.5, 2.5 Hz, 1H), 7.35 (d, J = 8.3 Hz, 1H), 7.17 (t, J = 7.5 Hz, 1H), 5.30 (s, 2H). ^{13}C NMR (151 MHz, DMSO-d_6) δ 166.33, 155.51, 138.46, 136.91, 133.20, 132.43, 131.45, 130.69, 130.12, 129.77, 129.10, 127.43, 125.46, 121.92, 114.10, 67.23. HPLC purity: 99.0%.

4.2.25 2-((5-fluoro-2-methylbenzyl)oxy)-N-(pyridin-3-yl)benzamide (33)

The title compound was obtained starting from **12** and **18k** according to the general procedure. White solid **33**, yield 63.3%, m.p 156.2-157.7^{o}C. ESI-MS(*m/z*):337.2[M+H]$^{+}$. HRMS (ESI) of $C_{20}H_{17}FN_2O_2$ [M+H]$^{+}$ calcd, 337.1347, found 337.1356. ^{1}H NMR (600 MHz, DMSO-d_6) δ 11.05 (d, J = 6.3 Hz, 1H), 9.21 (s, 1H), 8.59 (d, J = 5.3 Hz, 1H), 8.47 (d, J = 7.7 Hz, 1H), 7.90 (dt, J = 9.1, 4.7 Hz, 1H), 7.63 (dd, J = 7.5, 1.7 Hz, 1H), 7.60 – 7.55 (m, 1H), 7.36 (d, J = 8.4 Hz, 1H), 7.28 (dd, J = 10.0, 2.7 Hz, 1H), 7.23 (dd, J = 8.2, 6.0 Hz, 1H), 7.14 (t, J = 7.4 Hz, 1H), 7.02 (td, J = 8.5, 2.8 Hz, 1H), 5.24 (s, 2H), 2.28 (s, 3H). ^{13}C NMR (151 MHz, DMSO-d_6) δ 166.40, 161.74, 160.14, 155.84, 139.05, 138.28, 137.63, 134.51, 133.03, 132.16, 129.96, 127.13, 125.35, 121.49, 114.60, 114.06, 68.04, 18.06. HPLC purity: 98.7%.

4.2.26 2-((2,6-dimethylbenzyl)oxy)-N-(pyridin-3-yl)benzamide (36)

The title compound was obtained starting from **12** and **18p** according to the general procedure. White solid **36**, yield 78.4%, m.p 145.7-148.5^{o}C. ESI-MS(*m/z*):333.1[M+H]$^{+}$. HRMS (ESI) of $C_{21}H_{20}N_2O_2$ [M+H]$^{+}$ calcd, 333.1598, found 333.1603. ^{1}H NMR (400 MHz, DMSO-d_6) δ 11.07 (s, 1H), 9.08 (d, J = 1.8 Hz, 1H), 8.57 (d, J = 5.2 Hz, 1H), 8.30 (d, J = 8.6 Hz, 1H), 7.91 (dd, J = 8.5, 5.5 Hz, 1H), 7.58 (dd, J = 13.8, 4.6 Hz, 2H), 7.45 (d, J = 8.2 Hz, 1H), 7.11 (dd, J = 13.3, 7.1 Hz,

2H), 7.00 (d, *J* = 7.5 Hz, 2H), 5.18 (s, 2H), 2.31 (s, 6H). ^{13}C NMR (101 MHz, DMSO-d_6) δ 165.87, 156.20, 138.14, 137.93, 137.00, 133.47, 132.64, 132.39, 132.07, 129.35, 128.53, 128.05, 127.23, 124.73, 120.91, 113.94, 65.69, 19.17. HPLC purity: 98.6%.

4.2.27 2-((2,5-dimethoxybenzyl)oxy)-N-(pyridin-3-yl)benzamide (37)

The title compound was obtained starting from **12** and **18l** according to the general procedure. White solid **37**, yield 57.3%, m.p 108.2-110.5^{o}C. ESI-MS(*m/z*):365.1[M+H]$^{+}$. HRMS (ESI) of $C_{21}H_{20}N_2O_4$ [M+H]$^{+}$ calcd, 365.1496; found, 365.1495. ^{1}H NMR (400 MHz, DMSO-d_6) δ 10.38 (s, 1H), 8.65 (s, 1H), 8.26 (d, *J* = 4.1 Hz, 1H), 8.08 (d, *J* = 8.2 Hz, 1H), 7.72 (d, *J* = 7.4 Hz, 1H), 7.52 (t, *J* = 7.7 Hz, 1H), 7.34 (dd, *J* = 8.0, 4.7 Hz, 1H), 7.29 (d, *J* = 8.3 Hz, 1H), 7.11 (dd, *J* = 15.2, 4.9 Hz, 2H), 6.96 (d, *J* = 8.9 Hz, 1H), 6.86 (dd, *J* = 8.9, 2.6 Hz, 1H), 5.19 (s, 2H), 3.71 (s, 3H), 3.55 (s, 3H). ^{13}C NMR (101 MHz, DMSO-d_6) δ 164.71, 155.71, 153.07, 150.73, 144.41, 140.90, 135.56, 132.55, 129.98, 126.21, 124.99, 124.24, 123.62, 120.95, 114.91, 113.93, 113.37, 111.95, 65.56, 55.88, 55.15. HPLC purity: 99.1%.

4.2.28 2-((5-chloro-2-methoxybenzyl)oxy)-N-(pyridin-3-yl)benzamide (38)

The title compound was obtained starting from **12** and **18q** according to the general procedure. White solid **38**, yield 48.6%, m.p 119.0-122.8^{o}C. ESI-MS(*m/z*):369.1[M+H]$^{+}$. HRMS (ESI) of $C_{20}H_{17}ClN_2O_3$ [M+H]$^{+}$ calcd, 369.1000, found 369.1003. ^{1}H NMR (400 MHz, DMSO-d_6) δ 10.39 (s, 1H), 8.74 (d, *J* = 2.2 Hz, 1H), 8.27 (dd, *J* = 4.7, 1.3 Hz, 1H), 8.11 (ddd, *J* = 8.3, 2.3, 1.5 Hz, 1H), 7.67 (dd, *J* = 7.6, 1.6 Hz, 1H), 7.56 – 7.48 (m, 2H), 7.38 – 7.31 (m, 2H), 7.27 (d, *J* = 8.3 Hz, 1H), 7.10 (t, *J* = 7.5 Hz, 1H), 7.04 (d, *J* = 8.8 Hz, 1H), 5.18 (s, 2H), 3.77 (s, 3H). ^{13}C NMR (101 MHz, DMSO-d_6) δ 164.90, 155.36, 155.22, 144.36, 140.88, 135.56,

132.33, 129.78, 128.70, 128.05, 126.41, 126.15, 124.89, 124.20, 123.61, 121.02, 113.28, 112.57, 64.70, 55.84. HPLC purity: 99.3%.

4.2.29 2-((5-chloro-2-(2-methoxyethoxy)benzyl)oxy)-N-(pyridin-3-yl)benzamide (39)

The title compound was obtained starting from **12** and **18x** according to the general procedure. White solid **39**, yield 39.4%, m.p 98.6-101.2^{o}C. ESI-MS(*m/z*):413.1[M+H]$^{+}$. HRMS (ESI) of $C_{22}H_{21}ClN_2O_4$ [M+H]$^{+}$ calcd, 413.1263, found, 413.1266. ^{1}H NMR (400 MHz, DMSO-d_6) δ 10.35 (s, 1H), 8.71 (d, J = 2.3 Hz, 1H), 8.27 (dd, J = 4.7, 1.4 Hz, 1H), 8.10 (ddd, J = 8.3, 2.4, 1.5 Hz, 1H), 7.69 (dd, J = 7.6, 1.7 Hz, 1H), 7.55 (d, J = 2.5 Hz, 1H), 7.53 – 7.49 (m, 1H), 7.37 – 7.34 (m, 1H), 7.32 (dd, J = 8.9, 2.6 Hz, 1H), 7.25 (d, J = 8.3 Hz, 1H), 7.12 (d, J = 7.5 Hz, 1H), 7.07 (d, J = 8.9 Hz, 1H), 5.19 (s, 2H), 4.11 (t, J = 4.4 Hz, 2H), 3.59 (t, J = 4.4 Hz, 2H), 3.21 (s, 3H). ^{13}C NMR (101 MHz, DMSO-d_6) δ 164.85, 155.50, 154.62, 144.35, 140.87, 135.58, 132.42, 129.89, 128.80, 128.29, 126.85, 126.19, 124.79, 124.50, 123.62, 121.06, 113.99, 113.26, 70.17, 68.10, 64.81, 58.23. HPLC purity: 98.5%.

4.2.30 2-((5-chloro-2-(3-methoxypropoxy)benzyl)oxy)-N-(pyridin-3-yl)benzamide (40)

The title compound was obtained starting from **12** and **18w** according to the general procedure. White solid **40**, yield 82.8%, m.p 95.2-97.4^{o}C. ESI-MS(*m/z*):427.2[M+H]$^{+}$. HRMS (ESI) of $C_{23}H_{23}ClN_2O_4$ [M+H]$^{+}$ calcd, 427.1419, found, 427.1432. ^{1}H NMR (400 MHz, DMSO-d_6) δ 10.36 (s, 1H), 8.67 (d, J = 2.3 Hz, 1H), 8.26 (dd, J = 4.7, 1.4 Hz, 1H), 8.12 – 8.06 (m, 1H), 7.70 (dd, J = 7.6, 1.7 Hz, 1H), 7.53 (dd, J = 12.3, 2.2 Hz, 2H), 7.37 – 7.30 (m, 2H), 7.28 (d, J = 8.3 Hz, 1H), 7.11 (t, J = 7.4 Hz, 1H), 7.05 (d, J = 8.8 Hz, 1H), 5.19 (s, 2H), 4.01 (t, J = 6.2

Hz, 2H), 3.36 (t, *J* = 6.2 Hz, 2H), 3.13 (s, 3H), 1.87 (m, 2H). ^{13}C NMR (101 MHz, DMSO-d_6) δ 164.71, 155.63, 154.73, 144.38, 140.87, 135.53, 132.50, 129.98, 128.89, 128.39, 126.63, 126.17, 124.56, 124.26, 123.60, 121.10, 113.55, 113.36, 68.32, 65.42, 65.06, 57.82, 28.73. HPLC purity: 98.6%.

4.2.31 2-((2-(4-chlorobutoxy)benzyl)oxy)-N-(pyridin-3-yl)benzamide (41)

The title compound was obtained starting from **12** and **18r** according to the general procedure. White solid **41**, yield 60.0%, m.p 127.4-128.1^{o}C. ESI-MS(*m/z*):411.2[M+H]$^{+}$. HRMS (ESI) of $C_{23}H_{23}ClN_2O_3$ [M+H]$^{+}$ calcd, 411.1470; found, 411.1481. ^{1}H NMR (400 MHz, DMSO-d_6) δ 10.96 (s, 1H), 9.15 (d, *J* = 1.8 Hz, 1H), 8.60 (d, *J* = 5.1 Hz, 1H), 8.40 (d, *J* = 8.7 Hz, 1H), 7.93 (dd, *J* = 8.5, 5.4 Hz, 1H), 7.72 (dd, *J* = 7.6, 1.7 Hz, 1H), 7.61 – 7.54 (m, 1H), 7.50 – 7.45 (m, 1H), 7.31 (dd, *J* = 10.2, 5.0 Hz, 2H), 7.13 (t, *J* = 7.3 Hz, 1H), 7.05 (d, *J* = 8.1 Hz, 1H), 6.91 (t, *J* = 7.3 Hz, 1H), 5.26 (s, 2H), 4.03 (t, *J* = 5.7 Hz, 2H), 3.64 (t, *J* = 6.1 Hz, 2H), 1.88 – 1.72 (m, 4H). ^{13}C NMR (101 MHz, DMSO-d_6) δ 165.32, 155.90, 137.92, 137.71, 133.36, 132.95, 132.81, 129.90, 129.42, 128.83, 126.73, 124.20, 123.66, 120.89, 120.28, 113.53, 111.76, 66.97, 65.67, 45.04, 28.70, 25.95. HPLC purity: 98.0%.

4.2.32 2-((2-((5-chloropentyl)oxy)benzyl)oxy)-N-(pyridin-3-yl)benzamide (42)

The title compound was obtained starting from **12** and **18s** according to the general procedure. White solid **42**, yield 57.0%, m.p 87.8-88.4^{o}C. ESI-MS(*m/z*):425.2[M+H]$^{+}$. HRMS (ESI) of $C_{24}H_{25}ClN_2O_3$ [M+H]$^{+}$ calcd, 425.1626, found 425.1636. ^{1}H NMR (400 MHz, DMSO-d_6) δ 10.95 (s, 1H), 9.14 (d, *J* = 1.7 Hz, 1H), 8.60 (d, *J* = 5.1 Hz, 1H), 8.39 (d, *J* = 9.2 Hz, 1H), 7.93 (dd, *J* = 8.5, 5.4 Hz, 1H), 7.73 (dd, *J* = 7.6, 1.6 Hz, 1H), 7.61 – 7.54 (m, 1H), 7.47 (d, *J* = 6.3 Hz, 1H), 7.32 (dd, *J* = 10.7, 4.8 Hz, 2H), 7.14 (t, *J* = 7.4 Hz, 1H), 7.05 (d, *J* = 8.1 Hz, 1H), 6.91 (t, *J* = 7.4 Hz, 1H), 5.26 (s, 2H), 3.99 (t, *J* = 6.2 Hz, 2H), 3.58 (t, *J* = 6.6 Hz, 2H), 1.76

– 1.62 (m, 4H), 1.52 – 1.42 (m, 2H). ^{13}C NMR (101 MHz, DMSO-d_6) δ 165.26, 155.98, 137.90, 137.70, 133.30, 132.99, 132.83, 129.94, 129.48, 128.89, 126.75, 124.17, 123.53, 120.90, 120.24, 113.52, 111.80, 67.47, 65.74, 45.13, 31.53, 27.76, 22.78. HPLC purity: 98.4%.

4.2.33 2-((2-((6-chlorohexyl)oxy)benzyl)oxy)-N-(pyridin-3-yl)benzamide (43)

The title compound was obtained starting from **12** and **18t** according to the general procedure. White solid **43**, yield 61.0%, m.p 113.7-115.4^{o}C. ESI-MS(*m/z*):439.2[M+H]$^{+}$. HRMS (ESI) of $C_{25}H_{27}ClN_2O_3$ [M+H]$^{+}$ calcd, 439.1783, found 439.1796. ^{1}H NMR (400 MHz, DMSO-d_6) δ 10.85 (s, 1H), 9.06 (d, J = 12.3 Hz, 1H), 8.56 (d, J = 5.2 Hz, 1H), 8.31 (d, J = 8.5 Hz, 1H), 7.87 (t, J = 9.5 Hz, 1H), 7.76 (d, J = 7.6 Hz, 1H), 7.62 – 7.55 (m, 1H), 7.48 (d, J = 7.4 Hz, 1H), 7.33 (t, J = 7.1 Hz, 2H), 7.14 (t, J = 7.5 Hz, 1H), 7.05 (d, J = 8.3 Hz, 1H), 6.92 (t, J = 7.4 Hz, 1H), 5.27 (s, 2H), 3.98 (t, J = 6.3 Hz, 2H), 3.57 (t, J = 6.6 Hz, 2H), 1.64 (dd, J = 13.1, 6.5 Hz, 4H), 1.43 – 1.31 (m, 4H). ^{13}C NMR (101 MHz, DMSO-d_6) δ 165.43, 156.08, 138.09, 137.05, 133.64, 133.11, 132.31, 130.04, 129.55, 129.00, 127.22, 124.25, 123.53, 120.95, 120.28, 113.60, 111.83, 67.61, 65.84, 45.28, 31.89, 28.43, 25.95, 24.73. HPLC purity: 99.2%.

4.2.34 2-((5-chloro-2-(hexyloxy)benzyl)oxy)-N-(pyridin-3-yl)benzamide (44)

The title compound was obtained starting from **12** and **18u** according to the general procedure. White solid **44**, yield 72.9%, m.p 155.3-158.0^{o}C. ESI-MS(*m/z*):439.2[M+H]$^{+}$. HRMS (ESI) of $C_{25}H_{27}ClN_2O_3$ [M+H]$^{+}$ calcd, 439.1783, found 439.1787. ^{1}H NMR (400 MHz, DMSO-d_6) δ 11.18 (s, 1H), 9.27 (d, J = 1.8 Hz, 1H), 8.64 (d, J = 5.4 Hz, 1H), 8.56 (d, J = 8.7 Hz, 1H), 8.00 (dd, J = 8.6, 5.5 Hz, 1H), 7.65 (dd, J = 7.6, 1.5 Hz, 1H), 7.58 – 7.51 (m, 1H), 7.45 (d, J = 2.6 Hz, 1H), 7.26 (dd, J = 12.2, 5.7 Hz, 2H), 7.11 (t, J = 7.5 Hz, 1H), 7.02 (d, J = 8.8 Hz, 1H), 5.17 (s,

2H), 3.95 (t, *J* = 6.4 Hz, 2H), 1.68 – 1.58 (m, 2H), 1.32 (dd, *J* = 14.4, 7.1 Hz, 2H), 1.22 (dt, *J* = 7.1, 4.7 Hz, 4H), 0.80 (t, *J* = 7.0 Hz, 3H). ^{13}C NMR (101 MHz, $CDCl_3$) δ 165.73, 155.53, 154.48, 138.23, 133.81, 132.91, 129.82, 128.54, 127.74, 127.38, 126.68, 124.20, 123.96, 121.09, 113.45, 113.35, 68.20, 64.69, 30.87, 28.38, 25.05, 21.97, 13.82. HPLC purity: 98.0%.

4.2.35 2-((5-chloro-2-(heptyloxy)benzyl)oxy)-N-(pyridin-3-yl)benzamide (45)

The title compound was obtained starting from **12** and **18v** according to the general procedure. White solid **45**, yield 64.0%, m.p 156.9-159.2^{o}C. ESI-MS(*m/z*):453.2$[M+H]^+$. HRMS (ESI) of $C_{26}H_{29}ClN_2O_3$ $[M+H]^+$ calcd, 453.1939, found 453.1942. ^{1}H NMR (400 MHz, DMSO-d_6) δ 11.16 (s, 1H), 9.26 (d, *J* = 2.0 Hz, 1H), 8.64 (d, *J* = 5.3 Hz, 1H), 8.54 (d, *J* = 8.7 Hz, 1H), 7.99 (dd, *J* = 8.6, 5.5 Hz, 1H), 7.66 (dd, *J* = 7.6, 1.6 Hz, 1H), 7.58 – 7.52 (m, 1H), 7.46 (d, *J* = 2.6 Hz, 1H), 7.26 (dd, *J* = 12.4, 5.8 Hz, 2H), 7.12 (t, *J* = 7.5 Hz, 1H), 7.02 (d, *J* = 8.9 Hz, 1H), 5.17 (s, 2H), 3.95 (t, *J* = 6.4 Hz, 2H), 1.69 – 1.57 (m, 2H), 1.38 – 1.28 (m, 2H), 1.27 – 1.11 (m, 6H), 0.80 (t, *J* = 6.9 Hz, 3H). ^{13}C NMR (151 MHz, DMSO-*d*6) δ 165.68, 155.61, 154.57, 138.18, 137.18, 133.54, 132.92, 132.47, 129.87, 128.60, 127.84, 127.24, 126.72, 124.21, 124.02, 121.13, 113.54, 113.41, 68.26, 64.80, 31.13, 28.45, 28.33, 25.34, 21.96, 13.90. HPLC purity: 98.2%.

4.2.36 General procedure for the preparation of 23, 34 and 35

To a solution of Ph_3P (0.20 g, 0.75 mmol) and DEAD (0.75 mmol) in anhydrous THF (10 ml) was added **12** (0.5 mmol) and **17o** or **17p** or **17q** (0.55 mmol) at 0 ^{o}C. The reaction mixture was stirred at room temperature for 2.0 h and then evaporated the solvent. The residue was purified by flash chromatograph eluting with ethyl acetate/petroleum ether (1:2, *v*: *v*) to afford **23**, **34**, and **35**.

4.2.37 N-(pyridin-3-yl)-2-((2-(trifluoromethyl)benzyl)oxy)benzamide (23)

The title compound was obtained starting from **12** and **17o** according to the general procedure. White solid **23**, yield 43.0%, m.p 73.6-75.1^{o}C. ESI-MS(*m/z*):373.1[M+H]$^{+}$. HRMS (ESI) of $C_{20}H_{15}F_3N_2O_2$ [M+H]$^{+}$ calcd, 373.1158, found 373.1159. ^{1}H NMR (400 MHz, DMSO-d_6) δ 10.37 (s, 1H), 8.67 (d, J = 2.4 Hz, 1H), 8.28 (dd, J = 4.7, 1.4 Hz, 1H), 8.13 – 8.07 (m, 1H), 7.88 (d, J = 7.6 Hz, 1H), 7.79 (d, J = 7.6 Hz, 1H), 7.71 – 7.61 (m, 2H), 7.61 – 7.52 (m, 2H), 7.36 (dd, J = 8.3, 4.7 Hz, 1H), 7.27 (d, J = 8.3 Hz, 1H), 7.14 (t, J = 7.4 Hz, 1H), 5.40 (s, 2H). ^{13}C NMR (101 MHz, DMSO-d_6) δ 165.46, 155.65, 144.88, 141.37, 136.12, 135.09, 133.25, 132.76, 130.44, 130.24, 129.23, 126.65, 125.78, 124.10, 121.74, 113.72, 67.13. HPLC purity: 98.9%.

4.2.38 2-((5-chloro-2-methylbenzyl)oxy)-N-(pyridin-3-yl)benzamide (34)

The title compound was obtained starting from **12** and **17p** according to the general procedure. White solid **34**, yield 76.9%, m.p 177.8-178.9^{o}C. ESI-MS(*m/z*):353.1[M+H]$^{+}$. HRMS (ESI) of $C_{20}H_{17}ClN_2O_2$ [M+H]$^{+}$ calcd, 353.1051, found 353.1052. ^{1}H NMR (400 MHz, DMSO-d_6) δ 11.20 (s, 1H), 9.26 (s, 1H), 8.62 (d, J = 5.3 Hz, 1H), 8.54 (d, J = 8.6 Hz, 1H), 7.97 (dd, J = 8.5, 5.5 Hz, 1H), 7.60 (d, J = 7.6 Hz, 1H), 7.55 (d, J = 7.4 Hz, 1H), 7.47 (s, 1H), 7.36 (d, J = 8.4 Hz, 1H), 7.24 – 7.17 (m, 2H), 7.12 (t, J = 7.5 Hz, 1H), 5.20 (s, 2H), 2.27 (s, 3H). ^{13}C NMR (101 MHz, $CDCl_3$) δ 166.05, 155.26, 138.13, 137.17, 134.56, 132.56, 131.72, 130.20, 129.41, 127.26, 126.70, 124.85, 120.99, 113.50, 67.22, 17.75. HPLC purity: 99.2%.

4.2.39 2-((3-chloro-2-methylbenzyl)oxy)-N-(pyridin-3-yl)benzamide (35)

The title compound was obtained starting from **12** and **17q** according to the general procedure. White solid **35**, yield 28.4%, m.p 98.6-100.5^{o}C. ESI-MS(*m/z*):353.1[M+H]$^{+}$. HRMS (ESI) of $C_{20}H_{17}ClN_2O_2$ [M+H]$^{+}$ calcd, 353.1051;

found, 353.1062. ^{1}H NMR (400 MHz, DMSO-d_6) δ 10.37 (s, 1H), 9.00 (s, 1H), 8.66 (d, J = 1.9 Hz, 1H), 8.26 (d, J = 4.1 Hz, 1H), 8.07 (d, J = 8.7 Hz, 1H), 7.64 – 7.57 (m, 2H), 7.39 (d, J = 7.9 Hz, 1H), 7.37 – 7.31 (m, 2H), 7.15 (t, J = 7.8 Hz, 1H), 7.09 (t, J = 7.4 Hz, 1H), 5.27 (s, 2H), 2.33 (s, 3H). ^{13}C NMR (101 MHz, DMSO-d_6) δ 165.12, 155.21, 144.34, 140.77, 136.98, 134.13, 133.88, 131.99, 129.43, 128.77, 127.31, 126.98, 126.03, 125.36, 123.60, 120.92, 113.45, 68.50, 14.49. HPLC purity: 99.5%.

4.3 The determination of SMS inhibitory activities in vitro.

The general method is detailed as follows. Various concentrations of inhibitor were firstly added into the SMS enzyme and pre-incubated. Subsequently, the substrates, C6-NBD-Ceramide and DMPC were added and whirled. After incubating at 37 ^{o}C, the reactions were quenched with anhydrous ethanol. Then the mixture was centrifuged at 10000 rpm for 10 minutes to have the supernatant collected for TLC or HPLC test according to the reported method [47-49]. All values were averages of three parallel trials. The IC_{50} values were calculated by the "Nonlinear regression(curve fit)-log(inhibitor) vs. response" function of GraphPad Prism software (version 5.01, GraphPad Software, Inc.)

4.3.1 The determination of SMS2 inhibitory activities against SMS2 over-expressed insect cell lysate by 2-benzyloxybenzamides in vitro.

SMS2 over-expressed insect cell homogenates was kindly provided by Dr. Yanhui Xu's lab, Institute of Biomedical Sciences, Shanghai Medical College of Fudan University, China. The SMS2 enzyme was over-expressed in H5 insect cell and the lysate of cell pellet was directly used in the assay. Buffer 1 (0.25 M sucrose, 50 mM Tris·HCl, pH 7.4, 1 mM EDTA) was prepared for the storage of SMS enzyme. Buffer 2 (100 mM HEPES, pH 7.4, 30 mM $MnCl_2$, 3 % BSA) was prepared for the assay of SMS2 inhibitory activities.

294 μl test mixture, which contained 4 μl SMS2 in buffer 1 (equivalent to 2 μg total

protein), 10 μl DMSO solution of 2-benzyloxybenzamides, 30 μl buffer 2 and 250 μl water, was incubated at 37ºC for 30 minutes. Then 3 μl C6-NBD-Cer in ethanol (1.16 mM) and 3 μl DMPC in ethanol (40 mM) were added as substrates into the above-mentioned test system. Subsequently, the total of 300 μl mixture was incubated at 37°C for an additional 2.0 h. The test system was quenched by 600 μl ethanol. The following procedure is conducted according to the general method.

4.3.2 The determination of inhibitory activities against purified SMS1 and SMS2 by Ly93 in vitro.

The stock DDM solution of purified SMS1 has a protein content of 1.5 μg/μL. The stock DDM solution of purified SMS2 has a protein content of 1.6 μg/μL. 1 μl DMSO solution of each Ly93 concentration was added to 80 μl diluted solution of SMS1 (0.8 μl purified SMS1 stock solution in 79.2 μl DDM buffer) or SMS2 (0.03 μl purified SMS2 stock solution in 79.97 μl DDM buffer). After 5-minute pre-incubation at room temperature, 20 μl DDM solution of the two substrates, C6-NBD-Ceramide (1 μl, 1.16 mmol/L DMSO solution) and DMPC (1 μl, 40 mmol/L anhydrous ethanol solution), were added and whirled. After incubating at 37 ^{o}C for 30 minutes, the reaction was quenched with 200 μl of anhydrous ethanol. The following procedure is conducted according to the general method.

4.3.3 The determination of SMS activities in macrophages and apoE KO mice livers.

Bone marrow-derived macrophages were obtained from femurs of 8-week old male C57BL/6J mice as reported [50]. Bone marrow-derived macrophages or apoE KO mice livers (200 mg/ml, the weight of livers/volume of homogenate buffer) were homogenized in a homogenate buffer (50 mM Tris-HCl, pH 7.4, 1 mM EDTA, and 250 mM sucrose). Subsequently, C6-NBD-Ceramide and DMPC were added into the

homogenate and whirled. The homogenate derived from macrophages and apoE KO mice livers were respectively detected the SMS activities according to the general method.

4.4 The molecular modeling study.

As to the high sequence homology shared by *h*SMS1 and *h*SMS2 [16], especially in the catalytic site [50], the *h*SMS2 homology model was built from the previously reported three-dimensional model of human sphingomyelin synthase 1 (*h*SMS1) [31, 34]. Sequence alignment and structure generation were conducted in the Prime module of Schrödinger software package (Schrödinger, L. Schrödinger Software Suite. New York: Schrödinger, LLC 2011) with default settings (unpublished work). The docking studies were also carried out by Schrödinger software package. The newly built *h*SMS2 homology model and the previously reported *h*SMS1 model [34] were used as the receptor protein structures. All hydrogen atoms of the proteins were added by standard protein preparation protocol within Maestro, followed by energy minimization using OPLS 2005 force field. Restrained minimization was later performed on heavy atoms of the proteins with root-mean-square deviation (RMSD) converged to 0.3 Å. The structure of compound Ly93 was built and optimized by Maestro with default settings. Docking study of compound Ly93 was carried out using Glide with standard precision protocol. The binding conformation with the lowest score was selected to represent the predicted binding modes with *h*SMS1 and *h*SMS2, respectively.

4.5 Hepatocyte apoB-containing lipoprotein secretion measurement.

The method has been described previously [29, 51, 52].

4.6 Macrophage cholesterol efflux measurement.

Bone marrow-derived macrophages were treated by the various concentration of Ly93 for 17 hours. BMM were labeled with [^{3}H]-cholesterol carried by acetylated-LDL. After labeling, cells were washed with phosphate-buffered saline, equilibrated with DEME, 0.2 % bovine serum albumin for 1 hour, and incubated with

50 μg/ml HDL in 0.5 ml of DMEM, 0.2 % bovine serum albumin. The extracellular media were collected at 8 hours and centrifuged at 6,000 rpm for 10 minutes to remove residual cell debris and cholesterol crystals. Radioactivity in aliquots of supernatants was determined by liquid scintillation counting. The cells were finally lysed in 0.5 ml of 0.1 M sodium hydroxide, 0.1 % SDS, and the radioactivity in aliquots was determined. Cholesterol efflux was expressed as the percentage of the radioactivity released from the cells into the medium, relative to the total radioactivity in cells and medium.

4.7 Macrophage IL-6 and MCP-1 secretion measurements.

Bone marrow-derived macrophages were incubated with indicated various concentrations of Ly93 for 17 hours. After 50 ng/ml of LPS treated for 6 hours, IL-6 and MCP-1 in the culture medium were determined by ELISA described as the manufacturer's instruction.

4.8 Macrophage IκBα measurement.

Bone marrow-derived macrophages were incubated with various concentration of Ly93 for 17 hours before 1 μg/ml of LPS treatment. The cells were collected and total proteins were extracted by RIPA Lysis Buffer supplemented with 1 mM PMSF, 10 μg/ml aprotonin, 10 μg/ml leupeptin, 1 mM DTT, pH 7.4. Protein samples were detected by Western blot and probed with the following primary antibodies and secondary antibody: rabbit anti-mouse IκBα (Abcam) and β-actin antibody (Santa Cruz, CA, USA), followed by HRP-conjugated secondary antibody (Santa Cruz, CA, USA) and developed with ECL reagent (Beyotime Institute of Biotechnology, Shanghai).

4.9 Pharmacokinetic studies.

A total of twenty-four C57BL/6J male mice (six to eight-week-old), weighing approximately 20 g, were used for the experiment. The mice were starved for 12 h before the experiment and had free access to water. All mice were randomly divided into intragastric (i.g.) groups. Ly93 was prepared in a 10% DMSO/30%PEG-100/0.9%

NaCl aqueous solution [53]. Each mouse was administrated a single, 0.1 ml/10 g body weight dose (100, 50 and 25 mg/kg). Subsequently, blood samples (about 80 μl) were collected by a retro-orbital puncture at different time points, 5 min, 10 min, 20 min, 30 min, 1 h, 3 h, 5 h, and 8 h, after administration of Ly93. Plasma was separated immediately by centrifugation and stored at -80 °C until analysis.

Plasma samples and quantification of Ly93 were then analyzed by an HPLC-MS/MS method following protein precipitating. An aliquot (20 μl) of plasma was transferred to a test tube. Twenty microliters internal standard (500 ng/ml internal standard prepared in ethanol) and 100 μl of methanol were added for precipitating and the sample was vortex-mixed for one minute. The mixture was subsequently centrifuged at 12,000 rpm for 10 min at 4 °C. The upper layer of 50 μl was transferred to a polypropylene tube and further diluted with 50 μl water. Then 10 μl of supernatant fluid was injected into the LC-MS/MS system for analysis. Chromatographic separation of the supernatant was carried out on a Thermo Hypersil Gold C_{18} reversed-phase column (100 mm × 2.1 mm, 5 μm) equipped with a Hypersil Gold C_{18} guard column (10 mm × 2.1 mm, 5 μm) maintained at a temperature of 40 °C. The mobile phase consisted of 0.1% formic acid-methanol (25: 75, *v: v*) and was delivered at a flow rate of 0.3 ml/min. The temperature of the sample cooler in the auto-sampler was 4 °C. Analytes were detected by tandem mass spectrometry in positive electrospray ionization (ESI) mode using multiple reaction monitoring (MRM) with the transitions of *m*/*z* 333.2→214.2 for Ly93 and *m*/*z* 357.2→214.2 for IS. The temperature of the heater was maintained at 450 °C. A calibration curve was constructed and validated with spiked samples of rat or mouse plasma. The peak area ratios of analyte to the internal standard were linear over the concentration range tested, with all correlation coefficients (weighted least-square linear regression analyses) > 0.999. Accuracy (deviation of the analyzed quality-control samples from nominal values) was within ± 15% over the entire range of the calibration curve, and the precision (coefficient of variation of repeated measurements of the quality-control

samples) was < 15%. Representative mass spectra and chromatograms for Ly93 and internal standard (IS) are shown in **Supplementary Figure 3**. The pharmacokinetic profiles of the compounds were analyzed by standard noncompartmental procedures using Phoenix WinNonlin 6.2 (Pharsight Corporation, Mountain View, CA).

4.10 Analysis of plasma lipids and liver enzymes.

At the age of 20 weeks, the blood samples of three apoE KO mice groups were collected. The plasma lipids including SM, cholesterol, and triglyceride in these blood samples were measured according to the method that was reported previously [18, 54, 55]. Alanine aminotransferase (ALT) and aspartate aminotransferase (AST) were assessed using an automated biochemical analyzer (Hitachi 7080).

4.11 Flow cytometry analysis.

Single-cell suspensions obtained from blood of apoE KO mice were stained with appropriate antibodies in flow cytometry buffer (PBS). Neutrophile granulocyte, lymphocyte, monocyte, the ratio of CD4+ T cells /CD8+ T cells, CD11b+CD11c+ subset of dendritic cells, CD11b+Ly6C++ and Ly6G+cells (granulocytic Myeloid-derived suppressor cells, granulocytic MDSCs) were determined by BD FACS Aria(TM) III Flow Cytometry System (BD Biosciences).

4.12 Measuring atherosclerotic lesion size.

ApoE KO mice, on a 13-week Western-type diet, were sacrificed after 7 weeks of treatment with Ly93 (formulated for intragastric administration at 12.5 mg/kg/day or 40 mg/kg/day in 30 % PEG-400/10 % DMSO/0.9 % NaCl). The aortic arch was dissected and photographed as described [10, 14, 56]. Aortic root and *en face* assays were performed as follows. Aortic root assay: Sequential sections (4 µm thick) will be cut with a cryostat, stained with Hematoxylin and Eosin, and the mean area of lipid staining per section per animal from 6 sections will be calculated for each animal. Lesion areas will be quantified using Image-Pro Plus software. *En face* assay: The entire aorta will be isolated, the fatty streaks in the lumen stained with Oil Red O, and the percentage of tissue stained will be calculated for each animal using Image-Pro

Plus.

4.13 Immunostaining of macrophage in the plaques.

Sequential sections 4 μm thick were stained with the macrophage-specific antibody (MOMA). Immunohistochemistry staining for macrophages by monocyte/macrophage antibody-2 (MOMA-2) was performed as previously described [12, 57, 58]. Briefly, primary antibodies were incubated for 1 hour at room temperature in 3% serum matched to the species of the secondary antibodies. Biotinylated secondary antibodies were incubated for 30 minutes, followed by 45 minutes of horseradish peroxidase-conjugated streptavidin and visualization with diaminobenzidine. Nuclei were counterstained with hematoxylin. Staining areas were quantified with Image-Pro-Plus software.

4.14 Statistical analysis.

All of the data are typically expressed as means ± standard deviation of the mean (SD) and analyzed using GraphPad Prism 5. Data between two groups were analyzed by the unpaired, two-tailed Student's t test, and among multiple groups by ANOVA followed by the Dunnett test. A *P* value of less than 0.05 was considered statistically significant.

Author Contributions

X.J., N.C., D.Y. and L.Z. conceived and designed the research. Y.L., X.Q., Y.C., M.M., and Y.C. performed the chemistry experimental work and measured the enzymatic activities. Y.C., H.L. and Y.L. did the docking study. T.H., X.L., and S.H. implemented the pharmacokinetics and pharmacodynamics experiments. B.L., T.D., J.D., and M.W. accomplished the molecular biological experiments. X.J., N.C., D.Y., Y.L., T.H., and B.L. analyzed the data, discussed the results and wrote the manuscript. All the authors read and approved the final manuscript.

Acknowledgements

We gratefully acknowledge the financial support from the National Natural Science Foundation of China (Grants No.30973641; No.31100851), Key Scientific and Technological Project of Shanghai Science and Technology Committee (Grants No.14XD1400300 & 17431902300), the program for Shanghai Rising Star (15QA1400300), the 12th Graduate Innovation Foundation of Fudan University, and the open grant of the State Key Laboratory of Bio-organic and Natural Products Chemistry, CAS. We also owe great thanks to Prof. Yanhui Xu from Institute of Biomedical Sciences, Shanghai Medical College of Fudan University (Shanghai, China) and Prof. Yu Cao from Institute of Precision Medicine, the Ninth People's Hospital, School of Medicine, Shanghai Jiao Tong University (Shanghai, China) for the generous grant, with which did we succeed to have SMS2 over-expressed insect cell homogenates as well as purified SMS1 and SMS2 protein to evaluate our inhibitors.

Supplementary data

Competing financial interests: The authors declare no competing financial interests.

References

[1] Å. Nilsson, R.-D. Duan, Absorption and lipoprotein transport of sphingomyelin, Journal of Lipid Research, 47 (2006) 154-171.

[2] X.-C. Jiang, F. Paultre, T.A. Pearson, R.G. Reed, C.K. Francis, M. Lin, L. Berglund, A.R. Tall, Plasma sphingomyelin level as a risk factor for coronary artery disease, Arteriosclerosis, Thrombosis, and Vascular Biology, 20 (2000) 2614-2618.

[3] A. Schlitt, S. Blankenberg, D. Yan, H. von Gizycki, M. Buerke, K. Werdan, C. Bickel, K.J. Lackner, J. Meyer, H.J. Rupprecht, X.C. Jiang, Further evaluation of plasma sphingomyelin levels as a risk factor for coronary artery disease, Nutr Metab,

3 (2006) 5.

[4] T. Jeong, S.L. Schissel, I. Tabas, H.J. Pownall, A.R. Tall, X. Jiang, Increased sphingomyelin content of plasma lipoproteins in apolipoprotein E knockout mice reflects combined production and catabolic defects and enhances reactivity with mammalian sphingomyelinase, J Clin Invest, 101 (1998) 905-912.

[5] A.S. Plump, J.D. Smith, T. Hayek, K. Aalto-Setala, A. Walsh, J.G. Verstuyft, E.M. Rubin, J.L. Breslow, Severe hypercholesterolemia and atherosclerosis in apolipoprotein E-deficient mice created by homologous recombination in ES cells, Cell, 71 (1992) 343-353.

[6] J.L. Rodriguez, G.C. Ghiselli, D. Torreggiani, C.R. Sirtori, Very low density lipoproteins in normal and cholesterol-fed rabbits: lipid and protein composition and metabolism: Part 1. Chemical composition of very low density lipoproteins in rabbits, Atherosclerosis, 23 (1976) 73-83.

[7] Y. Fan, F. Shi, J. Liu, J. Dong, H.H. Bui, D.A. Peake, M.-S. Kuo, G. Cao, X.-C. Jiang, Selective Reduction in the Sphingomyelin Content of Atherogenic Lipoproteins Inhibits Their Retention in Murine Aortas and the Subsequent Development of Atherosclerosis, Arteriosclerosis, Thrombosis, and Vascular Biology, 30 (2010) 2114-2120.

[8] R. Ross, The pathogenesis of atherosclerosis: a perspective for the 1990s, Nature, 362 (1993) 801-809.

[9] P. Libby, Inflammation in atherosclerosis, Nature, 420 (2002) 868-874.

[10] J. Liu, C. Huan, M. Chakraborty, H. Zhang, D. Lu, M.-S. Kuo, G. Cao, X.-C. Jiang, Macrophage sphingomyelin synthase 2 deficiency decreases atherosclerosis in mice, Circulation research, 105 (2009) 295-303.

[11] Z. Li, Y. Fan, J. Liu, Y. Li, C. Huan, H.H. Bui, M.-S. Kuo, T.-S. Park, G. Cao, X.-C. Jiang, Impact of sphingomyelin synthase 1 deficiency on sphingolipid metabolism and atherosclerosis in mice, Arteriosclerosis, Thrombosis, and Vascular Biology, 32 (2012) 1577-1584.

[12] M. Chakraborty, C. Lou, C. Huan, M.S. Kuo, T.S. Park, G. Cao, X.C. Jiang, Myeloid cell-specific serine palmitoyltransferase subunit 2 haploinsufficiency reduces murine atherosclerosis, J Clin Invest, 123 (2013) 1784-1797.

[13] M. Chakraborty, X.C. Jiang, Sphingomyelin and its role in cellular signaling, Advances in experimental medicine and biology, 991 (2013) 1-14.

[14] M.R. Hojjati, Z. Li, H. Zhou, S. Tang, C. Huan, E. Ooi, S. Lu, X.-C. Jiang, Effect of myriocin on plasma sphingolipid metabolism and atherosclerosis in apoE-deficient mice, Journal of Biological Chemistry, 280 (2005) 10284-10289.

[15] T.-S. Park, R.L. Panek, S.B. Mueller, J.C. Hanselman, W.S. Rosebury, A.W. Robertson, E.K. Kindt, R. Homan, S.K. Karathanasis, M.D. Rekhter, Inhibition of sphingomyelin synthesis reduces atherogenesis in apolipoprotein E–knockout mice, Circulation, 110 (2004) 3465-3471.

[16] K. Huitema, J. van den Dikkenberg, J.F. Brouwers, J.C. Holthuis, Identification of a family of animal sphingomyelin synthases, The EMBO journal, 23

(2004) 33-44.

[17] S. Yamaoka, M. Miyaji, T. Kitano, H. Umehara, T. Okazaki, Expression cloning of a human cDNA restoring sphingomyelin synthesis and cell growth in sphingomyelin synthase-defective lymphoid cells, Journal of Biological Chemistry, 279 (2004) 18688-18693.

[18] J. Liu, H. Zhang, Z. Li, T.K. Hailemariam, M. Chakraborty, K. Jiang, D. Qiu, H.H. Bui, D.A. Peake, M.-S. Kuo, R. Wadgaonkar, G. Cao, X.-C. Jiang, Sphingomyelin Synthase 2 Is One of the Determinants for Plasma and Liver Sphingomyelin Levels in Mice, Arteriosclerosis, Thrombosis, and Vascular Biology, 29 (2009) 850-856.

[19] Z.-X. Jin, C.-R. Huang, L. Dong, S. Goda, T. Kawanami, T. Sawaki, T. Sakai, X.-P. Tong, Y. Masaki, T. Fukushima, Impaired TCR signaling through dysfunction of lipid rafts in sphingomyelin synthase 1 (SMS1)-knockdown T cells, International immunology, 20 (2008) 1427-1437.

[20] M. Yano, K. Watanabe, T. Yamamoto, K. Ikeda, T. Senokuchi, M. Lu, T. Kadomatsu, H. Tsukano, M. Ikawa, M. Okabe, Mitochondrial dysfunction and increased reactive oxygen species impair insulin secretion in sphingomyelin synthase 1-null mice, Journal of Biological Chemistry, 286 (2011) 3992-4002.

[21] M. Yano, T. Yamamoto, N. Nishimura, T. Gotoh, K. Watanabe, K. Ikeda, Y. Garan, R. Taguchi, K. Node, T. Okazaki, Y. Oike, Increased Oxidative Stress Impairs Adipose Tissue Function in Sphingomyelin Synthase 1 Null Mice, PLOS ONE, 8 (2013) e61380.

[22] J. Dong, J. Liu, B. Lou, Z. Li, X. Ye, M. Wu, X.-C. Jiang, Adenovirus-mediated overexpression of sphingomyelin synthases 1 and 2 increases the atherogenic potential in mice, Journal of Lipid Research, 47 (2006) 1307-1314.

[23] G. Sauer, E. Amtmann, K. Melber, A. Knapp, K. Muller, K. Hummel, A. Scherm, DNA and RNA virus species are inhibited by xanthates, a class of antiviral compounds with unique properties, Proceedings of the National Academy of Sciences of the United States of America, 81 (1984) 3263-3267.

[24] A. Gusain, J.F. Hatcher, R.M. Adibhatla, U.V. Wesley, R.J. Dempsey, Anti-proliferative effects of tricyclodecan-9-yl-xanthogenate (D609) involve ceramide and cell cycle inhibition, Molecular neurobiology, 45 (2012) 455-464.

[25] A. Meng, C. Luberto, P. Meier, A. Bai, X. Yang, Y.A. Hannun, D. Zhou, Sphingomyelin synthase as a potential target for D609-induced apoptosis in U937 human monocytic leukemia cells, Experimental cell research, 292 (2004) 385-392.

[26] A. Bai, G.P. Meier, Y. Wang, C. Luberto, Y.A. Hannun, D. Zhou, Prodrug modification increases potassium tricyclo [5.2.1.0(2, 6)]-decan-8-yl dithiocarbonate (D609) chemical stability and cytotoxicity against U937 leukemia cells, Journal of Pharmacology and Experimental Therapeutics, 309 (2004) 1051-1059.

[27] K. Zama, S. Mitsutake, K. Watanabe, T. Okazaki, Y. Igarashi, A sensitive cell-based method to screen for selective inhibitors of SMS1 or SMS2 using HPLC and a fluorescent substrate, Chemistry and physics of lipids, 165 (2012) 760-768.

[28] X. Deng, F. Lin, Y. Zhang, Y. Li, L. Zhou, B. Lou, Y. Li, J. Dong, T. Ding, X. Jiang, Identification of small molecule sphingomyelin synthase inhibitors, European Journal of Medicinal Chemistry, 73 (2014) 1-7.

[29] B. Lou, J. Dong, Y. Li, T. Ding, T. Bi, Y. Li, X. Deng, D. Ye, X.-C. Jiang, Pharmacologic Inhibition of Sphingomyelin Synthase (SMS) Activity Reduces Apolipoprotein-B Secretion from Hepatocytes and Attenuates Endotoxin-Mediated Macrophage Inflammation, PloS one, 9 (2014) 1-9.

[30] Y.-l. Li, X.-y. Qi, H. Jiang, X.-d. Deng, Y.-p. Dong, T.-b. Ding, L. Zhou, P. Men, Y. Chu, R.-x. Wang, Discovery, synthesis and biological evaluation of 2-(4-(N-phenethylsulfamoyl) phenoxy) acetamides (SAPAs) as novel sphingomyelin synthase 1 inhibitors, Bioorganic & medicinal chemistry, 23 (2015) 6173-6184.

[31] X.-Y. Qi, Y. Cao, Y.-L. Li, M.-G. Mo, L. Zhou, D.-Y. Ye, Discovery of the selective sphingomyelin synthase 2 inhibitors with the novel structure of oxazolopyridine, Bioorganic & Medicinal Chemistry Letters, 27 (2017) 3511-3515.

[32] R. Adachi, K. Ogawa, S.-i. Matsumoto, T. Satou, Y. Tanaka, J. Sakamoto, T. Nakahata, R. Okamoto, M. Kamaura, T. Kawamoto, Discovery and characterization of selective human sphingomyelin synthase 2 inhibitors, European Journal of Medicinal Chemistry, 136 (2017) 283-293.

[33] M. Mo, J. Yang, X.-C. Jiang, Y. Cao, J. Fei, Y. Chen, X. Qi, Y. Chu, L. Zhou, D. Ye, Discovery of 4-Benzyloxybenzo[d]isoxazole-3-amine Derivatives as Highly Selective and Orally Efficacious Human Sphingomyelin Synthase 2 Inhibitors that Reduce Chronic Inflammation in db/db Mice, Journal of Medicinal Chemistry, 61 (2018) 8241-8254.

[34] Y. Zhang, F. Lin, X. Deng, R. Wang, D. Ye, Molecular Modeling of the Three-Dimensional Structure of Human Sphingomyelin Synthase, Chinese Journal of Chemistry, 29 (2011) 1567-1575.

[35] S.H. Chen, G. Habib, C.Y. Yang, Z.W. Gu, B.R. Lee, S.A. Weng, S.R. Silberman, S.J. Cai, J.P. Deslypere, M. Rosseneu, et al., Apolipoprotein B-48 is the product of a messenger RNA with an organ-specific in-frame stop codon, Science, 238 (1987) 363-366.

[36] L.M. Powell, S.C. Wallis, R.J. Pease, Y.H. Edwards, T.J. Knott, J. Scott, A novel form of tissue-specific RNA processing produces apolipoprotein-B48 in intestine, Cell, 50 (1987) 831-840.

[37] A.V. Khera, M. Cuchel, M. de la Llera-Moya, A. Rodrigues, M.F. Burke, K. Jafri, B.C. French, J.A. Phillips, M.L. Mucksavage, R.L. Wilensky, E.R. Mohler, G.H. Rothblat, D.J. Rader, Cholesterol efflux capacity, high-density lipoprotein function, and atherosclerosis, The New England journal of medicine, 364 (2011) 127-135.

[38] S.S. Virani, V.R. Polsani, V. Nambi, Novel markers of inflammation in atherosclerosis, Current atherosclerosis reports, 10 (2008) 164-170.

[39] E.A. Biessen, J.C. Sluimer, Staging lymphocyte presence in human atherosclerosis: a tale told by numbers, Journal of the American Heart Association, 4 (2015).

[40] C.C. Hedrick, Lymphocytes in atherosclerosis, Arterioscler Thromb Vasc Biol, 35 (2015) 253-257.

[41] J. Zhou, P.C. Dimayuga, X. Zhao, J. Yano, W.M. Lio, P. Trinidad, T. Honjo, B. Cercek, P.K. Shah, K.Y. Chyu, CD8(+)CD25(+) T cells reduce atherosclerosis in apoE(-/-) mice, Biochemical and biophysical research communications, 443 (2014) 864-870.

[42] J. Abbasian, D. Mahmud, N. Mahmud, S. Chunduri, H. Araki, P. Reddy, R. Hoffman, M. Arpinati, J.L. Ferrara, D. Rondelli, Allogeneic T cells induce rapid CD34+ cell differentiation into CD11c+CD86+ cells with direct and indirect antigen-presenting function, Blood, 108 (2006) 203-208.

[43] K.E. Paulson, S.N. Zhu, M. Chen, S. Nurmohamed, J. Jongstra-Bilen, M.I. Cybulsky, Resident intimal dendritic cells accumulate lipid and contribute to the initiation of atherosclerosis, Circ Res, 106 (2010) 383-390.

[44] H. Wu, R.M. Gower, H. Wang, X.Y. Perrard, R. Ma, D.C. Bullard, A.R. Burns, A. Paul, C.W. Smith, S.I. Simon, C.M. Ballantyne, Functional role of CD11c+ monocytes in atherogenesis associated with hypercholesterolemia, Circulation, 119 (2009) 2708-2717.

[45] E. Kallberg, M. Stenstrom, D. Liberg, F. Ivars, T. Leanderson, CD11b+Ly6C++Ly6G- cells show distinct function in mice with chronic inflammation or tumor burden, BMC immunology, 13 (2012) 69.

[46] J. Sarkar, S. Chaudhary, S.H. Jassim, O. Ozturk, W. Chamon, B. Ganesh, S. Tibrewal, S. Gandhi, Y.S. Byun, J. Hallak, D.L. Mahmud, N. Mahmud, D. Rondelli, S. Jain, CD11b+GR1+ myeloid cells secrete NGF and promote trigeminal ganglion neurite growth: implications for corneal nerve regeneration, Investigative ophthalmology & visual science, 54 (2013) 5920-5936.

[47] X. Deng, H. Sun, X. Gao, H. Gong, W. Lu, Y. Chu, L. Zhou, D. Ye, Development, validation, and application of a novel method for mammalian sphingomyelin synthase activity measurement, Analytical Letters, 45 (2012) 1581-1589.

[48] Z. Li, T.K. Hailemariam, H. Zhou, Y. Li, D.C. Duckworth, D.A. Peake, Y. Zhang, M.-S. Kuo, G. Cao, X.-C. Jiang, Inhibition of sphingomyelin synthase (SMS) affects intracellular sphingomyelin accumulation and plasma membrane lipid organization, Biochimica et Biophysica Acta (BBA)-Molecular and Cell Biology of Lipids, 1771 (2007) 1186-1194.

[49] T. Huang, X. Li, S. Hu, B. Zhao, P. Chen, X. Liu, D. Ye, N. Cheng, Analysis of Fluorescent Ceramide and Sphingomyelin Analogs: A Novel Approach for in Vivo Monitoring of Sphingomyelin Synthase Activity, Lipids, 49 (2014) 1071-1079.

[50] C. Yeang, S. Varshney, R. Wang, Y. Zhang, D. Ye, X.-C. Jiang, The domain responsible for sphingomyelin synthase (SMS) activity, Biochimica et Biophysica Acta (BBA)-Molecular and Cell Biology of Lipids, 1781 (2008) 610-617.

[51] A. Mohammadi, J. Macri, R. Newton, T. Romain, D. Dulay, K. Adeli, Effects of atorvastatin on the intracellular stability and secretion of apolipoprotein B

in HepG2 cells, Arteriosclerosis, thrombosis, and vascular biology, 18 (1998) 783-793.

[52] X.-C. Jiang, S. Qin, C. Qiao, K. Kawano, M. Lin, A. Skold, X. Xiao, A.R. Tall, Apolipoprotein B secretion and atherosclerosis are decreased in mice with phospholipid-transfer protein deficiency, Nature medicine, 7 (2001) 847-852.

[53] K.H. Kolb, G. Jaenicke, M. Kramer, P.E. Schulze, Absorption, distribution and elimination of labeled dimethyl sulfoxide in man and animals, Annals of the New York Academy of Sciences, 141 (1967) 85-95.

[54] R. Ying, Y. Yuan, Y.F. Qin, D. Tian, L. Feng, Z.G. Guo, Y.X. Sun, M.X. Li, The combination of L-4F and simvastatin stimulate cholesterol efflux and related proteins expressions to reduce atherosclerotic lesions in apoE knockout mice, Lipids in health and disease, 12 (2013) 180.

[55] E.E. Mulvihill, J.M. Assini, B.G. Sutherland, A.S. DiMattia, M. Khami, J.B. Koppes, C.G. Sawyez, S.C. Whitman, M.W. Huff, Naringenin decreases progression of atherosclerosis by improving dyslipidemia in high-fat-fed low-density lipoprotein receptor-null mice, Arterioscler Thromb Vasc Biol, 30 (2010) 742-748.

[56] R. Liu, J. Iqbal, C. Yeang, D.Q. Wang, M.M. Hussain, X.C. Jiang, Phospholipid transfer protein-deficient mice absorb less cholesterol, Arterioscler Thromb Vasc Biol, 27 (2007) 2014-2021.

[57] L. Rogers, S. Burchat, J. Gage, M. Hasu, M. Thabet, L. Willcox, T.A. Ramsamy, S.C. Whitman, Deficiency of invariant V alpha 14 natural killer T cells decreases atherosclerosis in LDL receptor null mice, Cardiovascular research, 78 (2008) 167-174.

[58] J. Li, X. Han, J. Jiang, R. Zhong, G.M. Williams, J.G. Pickering, L.H. Chow, Vascular smooth muscle cells of recipient origin mediate intimal expansion after aortic allotransplantation in mice, The American journal of pathology, 158 (2001) 1943-1947.

Legends

Fig 1. Chemical structures of reported sphingomyelin synthase inhibitors.

Fig 2. The design strategy and SAR study of 2-benzyloxybenzamides as novel SMS2 inhibitors.

Fig 3. The inhibitory activities of Ly93 against purified SMS1 and SMS2 *in vitro*. (A) The inhibitory activity of Ly93 against purified SMS1 enzyme *in vitro*. (B)

The inhibitory activity of Ly93 against purified SMS2 enzyme *in vitro*. The results were expressed as percent of SMS1 or SMS2 activities in vehicle groups in which there is no inhibitor. (C) The dose-dependent inhibitory activities of Ly93 against purified SMS1 and SMS2 enzyme respectively *in vitro*. The IC_{50} value of D2 toward purified SMS2 was 20.9 μM. The inhibitory rate of D2 toward purified SMS1 was 57 % at the concentration of 100 μM. The IC_{50} value of Ly93 toward SMS1 was tested with ten concentrations. The IC_{50} value of Ly93 toward SMS2 was tested with eight concentrations. Values were shown in means ± SD, $n = 3$.

Fig 4. The molecular docking results of Ly93 with *h*SMS2 and *h*SMS1. (A) The binding mode of Ly93 with *h*SMS2. (B) The overlay map of binding modes of Ly93 with *h*SMS1 (yellow) and *h*SMS2 (red). The ribbons in colors stand for the six transmembrane (TM1-TM6) of *h*SMS2 and *h*SMS1. Carbon, oxygen, nitrogen, and hydrogen atoms of the Ly93 molecule are colored green, red, blue and gray, respectively.

Fig 5. The biological effects of Ly93 on the apoB secretion from Huh7 cells, intracellular SMS activity and cholesterol efflux in macrophages. (A) The effect of Ly93 on the apoB-containing particle secretion from Huh7 cells. Huh7 cells were treated by Ly93 for 17 h and then were labeled with [^{35}S]-methionine in the presence of vehicle or Ly93 for 2 hours. The medium was collected to detect [^{35}S]-apoB and the quantitation was displayed. (B) Ly93 inhibits macrophage lysate SMS activity in a dose-dependent manner. (C) Ly93 treatment significantly increased macrophage cholesterol efflux toward HDL. Values are mean ± SD, $n = 5$. *$P < 0.05$, **$P < 0.01$, ***$P < 0.001$.

Fig 6. The *in vitro* inhibitory activities of Ly93 against the LPS-mediated pro-inflammatory cytokine and chemokine secretion in macrophages. (A) IL-6 secreted by macrophages in culture medium after LPS (10 ng/ml for 16 h) treatment. (B) Western blot of IκB after LPS treatment (insert) and the quantitation was displayed. (C) MCP-1 production in macrophages induced by LPS. Values are mean ±

SD, $n = 7$. *$P < 0.05$, **$P < 0.01$.

Fig 7. The pharmacokinetics of Ly93. (A) Plasma concentration-time profile of Ly93. (B) The correlation between Ly93 $AUC_{0\text{-}8h}$ and dose from 25 to 100 mg/kg after i.g. administration. Values are mean ± SD, $n = 6$.

Fig 8. The effects on plasma SM concentration and liver enzymes by the treatment of Ly93 *in vivo*. (A) Plasma SM levels at day 0, 3 and 7 after Ly93 (i.g., 100 mg/kg) treatment once daily for 7 days ($n = 10$). (B) Ly93 distribution in blood and liver measured at day 7 after Ly93 (i.g., 100 mg/kg) treatment once daily for 7 days ($n = 5$). (C) AST and ALT levels at day 7 after a daily application of Ly93 (i.g., 100 mg/kg) ($n = 10$). Values are mean ± SD, **$P < 0.01$.

Fig 9. The liver SMS activities and SM levels in Ly93-treated apoE KO mice. (A) SMS activity in apoE KO mice liver after Ly93 treatment. (B) Plasma SM levels in apoE KO mice after Ly93 treatment. Low dose: 12.5 mg/kg, i.g., High dose: 40 mg/kg, i.g.. Values are mean ± SD, $n = 10$. *$P < 0.05$, **$P < 0.01$.

Fig 10. The blood cell analysis by flow cytometry in apoE KO mice after Ly93 treatment. (A) Representatives of the analysis of blood neutrophile granulocytes (NG), lymphocytes and monocytes in vehicle and Ly93 treated animals. (B-C) Quantitative display of gated lymphocytes and monocytes. (D) Representatives of the analysis of blood CD4+ T cells and CD8+ T cells. (E) Quantitative display of the ratio of CD4+ and CD8+ T cells. (F) Representatives of the analysis of blood CD11b+CD11c+ dendritic cells. (G) Quantitative display of the percentage of the dendritic cells. (H) Representatives of the analysis of blood CD11b+Ly6c+Ly6G+ cells. (I) Quantitative display of CD11b+Ly6c+Ly6G+ cells. Values are mean ± SD, $n = 5$, *$P < 0.05$, **$P < 0.01$, ***$P < 0.001$.

Fig 11. The effects on the development of atherosclerosis in apoE KO mice with Ly93 treatment. 8-week-old apoE KO mice were fed with a high fat and cholesterol diet for 6 weeks, and then the mice in three groups were treated with vehicle (i.g.), low dose Ly93 (12.5 mg/kg, i.g.) and high dose Ly93 (40 mg/kg, i.g.) respectively every

day for 7 weeks. (A) Aortic arches with atherosclerotic plaques (red arrows). (B) *Enface* aortic plaque analysis after Oil Red O staining. (C) Quantitative display of *en faces* aortic plaque. (D) Aortic root assay for lesion areas after Hematoxylin and eosin staining. (E) Quantitative display of lesion areas in the aortic root. (F) Immunohistochemical staining of macrophage accumulation in lesions (shown as brown stained regions indicated by blue arrows). (G) Quantitative display of macrophage content. Quantifications were done by using Image J software. Six alternate sections (4 μm thick) sliced from paraffin-fixed aortic root tissues of each transplanted mouse were used for the analysis. Values are mean ± SD. $n = 9$, $^{*}P < 0.05$, $^{**}P < 0.01$.

Scheme 1. The synthetic route for 2-benzyloxybenzamides 6-11. Reagents and conditions: (a) K_2CO_3, acetone, rt; (b) 1) 4 M NaOH(aq), CH_3OH; 2) 2M HCl (aq); (c) 1) $SOCl_2$, Pyridine (cat.), reflux; 2) Pyridine, CH_2Cl_2, 0 ^{o}C to rt; (d) 1) EDCI, DMAP, CH_2Cl_2, 0 ^{o}C to rt; 2) HCl (aq, con.), EA.

Scheme 2. The synthetic route for 2-benzyloxybenzamides 19-45. Reagents and conditions: (a) K_2CO_3, CH_3CN, 60 ^{o}C; (b) K_2CO_3, acetone, rt; (c) K_2CO_3, DMF, 100 ^{o}C; (d) $NaBH_4$, C_2H_5OH, 0 ^{o}C to rt; (e) BH_3, THF, 0 ^{o}C to rt; (f) PBr_3, CH_2Cl_2, 0 ^{o}C to rt; (g) H_2, 10% Pd/C, CH_3OH, rt; (h) DEAD, Ph_3P, THF, 0 ^{o}C to rt.

Table 1. The SMS2 inhibitory activities of 2-benzyloxybenzamides 6-11 and 19-45.

Discovery, synthesis and anti-atherosclerotic activities of a novel selective sphingomyelin synthase 2 inhibitor

Yali Li [a,b,#], Taomin Huang [a,c,#], Bin Lou [a, #], Deyong Ye [a], Xiangyu Qi [a], Xiaoxia Li [a], Shuang Hu [a], Tingbo Ding [a], Yan Chen [a], Yang Cao [a], Mingguang Mo [a], Jibin Dong [a], Min Wei [a], Yong Chu [a], Huiti Li [a], Xian-Cheng Jiang [a,d,*], Nengneng Cheng [a,*], Lu Zhou [a,*]

[a] *School of Pharmacy, Fudan University, No.826, Zhangheng Rd., Shanghai 201203, China*

[b] *Institute for Agro-food Standards and Testing Technology, Shanghai Academy of Agricultural Sciences, No.1000, Jinqi Rd., Shanghai 201403, China*

[c] *Eye Ear Nose Throat Hospital, Fudan University, No. 83, Fenyang Rd., Shanghai 200031, China*

[d] *State University of New York Downstate Medical Center, Brooklyn, New York 11203, USA*

Highlights

- 2-Benzyloxybenzamides were discovered as novel SMS2 inhibitors.
- 33 compounds were synthesized and studied SMS2 inhibitory activities for SARs.
- Ly93 was a selective SMS2 inhibitor with > 1400-fold selectivity for SMS2 over SMS1.
- The *in vitro* assays were performed on Ly93 for the study on the mechanism of action.
- Ly93 exhibited significant anti-atherosclerotic activities in the apoE KO mice.